UPPSALA
UNIVERSITET

Underwater Electrical Connections and Remotely Operated Vehicles

FLORE REMOUIT

UURIE 349-16L
ISSN 0349-8352

Division of Electricity
Department of Engineering Sciences
Licentiate Thesis

Uppsala, 2016

Abstract

Remotely Operated Vehicles (ROVs) are underwater robots that perform different kind of operations, from observation to heavier tasks like drilling, carrying and pulling cables, etc. Those ROVs are costly and require skilled personal to operate it as well as equipment for transportation and deployment (boats, cranes, etc.).
The division for electricity at Uppsala University, is developing a wave energy converter (WEC) concept. The concept is based on a point-absorbing buoy with a directly driven linear generator placed on the seabed. Several units are connected to a marine substation that is located on the seabed, whose role is to collect and smooth the power absorbed from the waves and then bring it to the shore through one single cable.
Cable connection is a big challenge in the project because the WEC concept is small and many units are necessary to create a rentable farm. Nowadays this operation is performed by divers but using Observation Class ROV (OCROV) could be an interesting alternative since they are affordable at lower costs and easier to operate. Cable connection is however a heavy task and requires force that an OCROV does not have. It will need a docking system from which the vehicle will take its force. It would then go to the station, dock itself to this support plate, grab the cables and connect them together. This procedure cannot be done by the ROV operator because it requires accurate displacement and quick adjustment of the robot's behavior.
An autopilot was created in Matlab Simulink that consists of three units: the path following, the ROV, and the positioning unit. The first one uses the vehicle's position and computes the speed and heading to be applied on the ROV in order to guide it on the desired path. The second one contains a controller that will adapt the thrust of each propeller to the force needed to reach the desired heading and speed from the path following unit. It also contains the model of the ROV that computes its position and speed. The last unit consists of a Kalman filter that estimates the ROV position and will be used in case of delay or failure in the communication with the positioning sensors.
The autopilot model is used with a positioning system that utilizes green lasers and image processing. Two green lasers are used as fixed points in each camera picture and from their distance on the image, the actual distance between the ROV and the docking platform can be computed. In addition, optical odometry is used. The idea behind is to estimate how the ROV is behaving by evaluating the changes between two pictures of the camera. Those two systems, laser and odometry, work together in order to get more accurate results.
The laser system has so far been tested in air. The distance measurements gave interesting results with an error inferior to 3%, and angle measurements gave less than 10% error for a distance of one meter. One advantage with the system is that it gets more accurate as the vehicle gets closer to the docking point.
In addition to the ROV project, a review study was conducted on the variability of wave energy compared with other resources such as tidal, solar, and wind power. An analysis of the different tools and models that are used to forecast the power generation of those sources was done. There is a need for collaboration between the different areas because the future will aggregate those different sources to the grid and requires a unification of the models and methods.

Seuls l'art et la science élèvent
l'homme jusqu'à la divinité
L. van Beethoven

List of Papers

This thesis is based on the following papers, which are referred to in the text by their Roman numerals.

I **Remouit, F.**, Lopes, M., Pires, P., Sebastiao, L., Rahm, M. (2015) Automation of subsea connection for clusters of wave energy converters. *The 25th International Ocean and Polar Engineering Conference, ISOPE, Hawaii, USA*

II Parwal, A., **Remouit, F.,** Hong, Y., Francisco, F., Castellucci, V., Hai, L., Li, W., Lejerskog, E., Baudoin, A., Nasir, M., Chatzigiannakou, M., Haikonen, K., Ekström, R., Boström, C., Göteman, M., Waters, R., Svensson, O., Sundberg, J., Rahm, M., Engström, J., Savin, A., Leijon, M. (2015) Wave Energy Research at Uppsala University and The Lysekil Research Site, Sweden: A Status Update. *The 11th European Wave and Tidal Energy Conference, EWTEC, Nantes, France*

III **Remouit, F.**, Abrahamsson, J., Engström, J. (2016) Optical System for Underwater Positioning of Observation Class Remotely Operated Vehicle. *Accepted for publication at The 3rd Asian Wave and Tidal Energy Conference, AWTEC, Singapore*

IV **Remouit, F.**, Kamf, T., Abrahamsson, J., Engström, J. (2016) Thruster model for Observation Class Remotely Operated Vehicle. *Submitted to Journal of Ocean Engineering*

V Joakim Widén, J., Carpman, N., Castellucci, V., Lingfors, D., Olauson, J., **Remouit, F.**, Bergkvist, M., Grabbe, M., Waters, R. (2015) Variability assessment and forecasting of renewables: A review for solar, wind, wave and tidal resources. *Renewable and Sustainable Energy Review, 356–375.*

Contents

Abbreviations

Abbreviation	Description
ANN	Artificial Neural Network
AR	Auto-Regressive
CAD	Computer-Aided Design
DMC	Dry Mateable Connector
DOF	Degree Of freedom
GA	Genetic Algorithm
HF	High Frequency
k-NN	k-Nearest Neighbor
LCD	Liquid Crystal Display
LCOE	Levelized Cost of Electricity
LF	Low Frequency
LVMS	Low Voltage Marine Substation
MAE	Mean Absolute Error
MSROV	Mid-Sized Remotely Operated Vehicle
O&M	Operation and Maintenance
OCROV	Observation-Class Remotely Operated Vehicle
OpenCV	Open source Computer Vision
PI	Proportional Integrator
RANSAC	Random Sample Consensus
RFID	Radio frequency Identification
RMSE	Root Mean Square Error
ROV	Remotely Operated Vehicle
SURF	Speeded-Up Robust Features
UHF	Ultra-High Frequency
WCROV	Working-Class Remotely Operated Vehicle
WEC	Wave Energy Converter
WMC	Wet Mateable Connector

1. Introduction

1.1 Wave energy and cable connection

To be able to compete with other energy sources, offshore renewables must keep a low levelized cost of electricity (LCOE). It means that both investments and Operations and Maintenance (O&M) costs must reach a level that is competitive with Oil and Gas industry. Two components with significant impact on those costs are grid connection and power transmission. Depending on the location of the farm, and the amount of units, it can increase the LCOE up to 5c/kWh (see [1]). The chart below, presented in *Figure 1*, shows the typical cost breakdown by cost center for wave arrays.

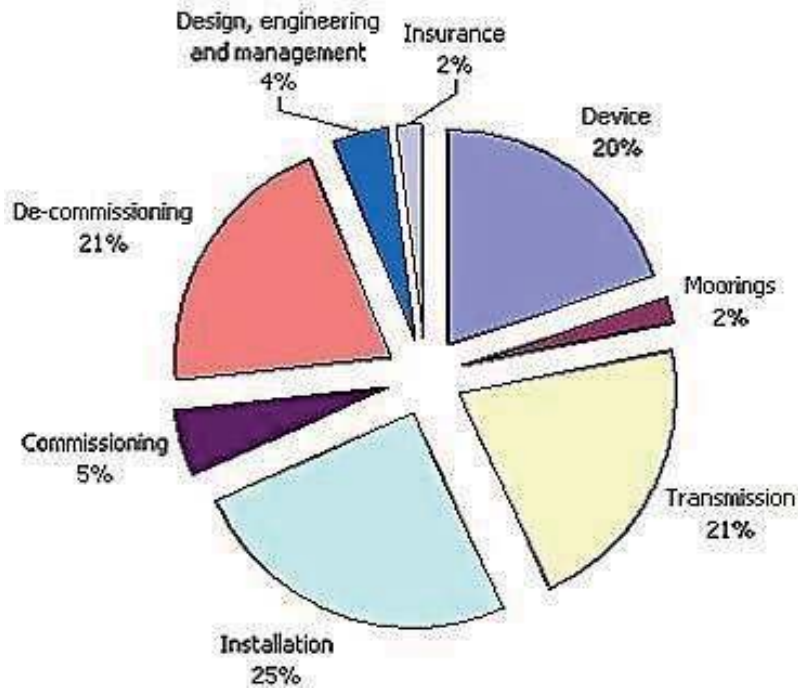

Figure 1. Division of the capital costs for a single wave energy converter (from [2]).

One can see in *Figure 1* that the costs for transmission are non-negligible, being 21% of the overall capital costs. One part of the installation is also related to cable connection. The main reason for high capital costs for grid connection is the price of the connectors.

There are basically two types of connectors for underwater physical connections. Wet mate connectors (or WMC's) can be used in submerged environments so the connection/disconnection can be performed directly subsea. Dry mate connectors (DMC's) can be submerged but have to be connected above water first and then assembled with the cable underwater. Using wet connectors is substantially more expensive than dry connectors, but underwater connectors is of high cost in any case. For more information on underwater connectors, see [3]–[6].

Another reason that increases the share of the grid connection in the LCOE of wave energy, is the cost of deployment that increases quickly and significantly with the amount of cables to connect. Repairing the cables is also a high budgetary item, since the cables are sensitive to the environment and the hazards are non-negligible (rocks and algae, currents and waves, fishes and marine mammals…).

1.2 Remotely Operated Vehicles

The deployment and connection of the cables can be done by divers or/and Remotely Operated Vehicles (ROVs). The latter are increasingly used for safety and cost purposes. ROVs can work longer and in deeper water than divers; they can also perform heavier tasks and work faster for certain operations for example repetitive ones.

ROV's are classified into different categories depending on their weight, size, ability, and power, as presented in [7]. We can overall consider three types, one is dedicated to observation (OCROV: Observation-Class Remotely Operated Vehicle), another is a usually deeper-rated version of the first type, or to perform light tasks with small tooling package (MSROV: Mid-Sized Remotely Operated Vehicle), and the last one is made for heavy work, with high power supply and strong tooling capabilities (WCROV: Work-Class Remotely Operated Vehicle). The Table 1 summarizes those three ROV categories.

Table 1. *Summary of ROV categories*

Category	Voltage	Mass	Typical depth rating	Launch Method	Thruster/Tooling
OCROV	DC voltage, 110/220V	Up to 100 kg	300 m	Manual	Electric
MSROV	DC/AC voltage, 440/480V	From 100 kg to 1000 kg	2000 m	Crane or A-frame	Electric or hydraulic
WCROV	AC voltage, 440/480V	>1000 kg	> 3000 m	A-frame	Hydraulic

MSROVs and WCROVs are the most commonly and widely used in the offshore industry. Their cost is significant, both for the device itself, but especially when taking into account the personal required to operate them, the boats used to transport them, and the equipment needed to use them (crane, batteries, winch…). It is hence hardly possible for a development company in offshore renewables to invest in such a robot.

1.3 The Lysekil Project

The division for electricity at Uppsala University operates a wave power project on the west coast of Sweden outside of Lysekil (8]–[13]). The wave energy converter (WEC) concept is based on a point-absorbing buoy with a directly driven linear generator placed on the seabed, as illustrated in *Figure 2*. There are many advantages with this technology, especially its small scale and modular characteristics, which makes it easily replaceable, without affecting the whole farm. It is indeed possible to adjust the amount of units to the available area and desired power output.

Figure 2. Graphical illustration of a WEC designed at Uppsala University.

However, due to this small scale, a large number of WECs is necessary to create significant power, and consequently the number of cables increases drastically. A marine substation has been developed whose role is to collect and smooth the power absorbed from the waves and then bring it to the shore through one single cable. It allows an aggregation of the power output between the different units, to decrease the number of sea cables used to transfer the power from the farm to the grid onshore, and to reduce electrical transmission losses. The current Low Voltage Marine Substation (LVMS) can be seen in *Figure 3*, and more information can be found in [8]. The substation is placed on the seabed to be protected from harsh weather.

Figure 3. The substation at Uppsala University

In order to decrease the budget of the connections within the Lysekil project the choice was made to use DMC's instead of WMC's, combined with an air pocket. The basic idea of the air-pocket solution is to create an artificial "dry environment" underwater to enable dry connection subsea and not above the water level. For this purpose, four boxes are fixed to the substation, each of them surrounding seven outputs used to connect the WECs cables, as shown in *Figure 4* and *Figure 5*. The space underneath the boxes is open to allow pressurized air to come in and for the connectors to enter the box. These boxes are designed to be used by divers but a small ROV could also perform those connection (and disconnection) operations with suitable tools and equipment.

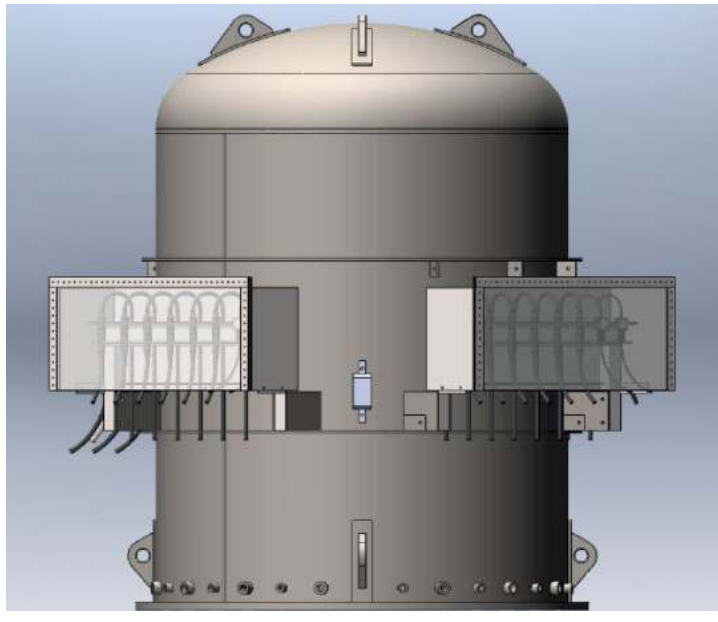

Figure 4. CAD file of the LVMS with its air pockets for dry connections

Figure 5. The connectors inside the air pocket.

1.4 Variability assessment and forecasting of wave energy

One characteristic of wave energy, as of many renewable energy resources, is its variability in time and space, which requires a forecast of the power generated and transmitted to the grid. With solar, wind, and tidal energies, that vary differently, are available at various times and places, depending on several factors (location of the farm, season, time of the day, weather, etc.), their integration into the grid is a challenge, and especially when integrating them all together. In this matter the research areas are at different stages and use different models to understand the variability in time of the output power and to forecast accurately the power generation. However there is a need for coordination between the different resources.

1.5 Aim of the Thesis

This thesis is studying the possibilities to use OCROVs to perform underwater electrical connections as an alternative to WCROVs and heavy O&M equipment. An OCROV is light and easy to operate, but lacks the thrust and force to perform cable connections (hence the name Observation Class ROV).

One solution to the lack of power is for the ROV to be equipped with different tools and modules that will mitigate its limited capabilities. In particular, it is necessary for the ROV to use force from a support structure as a docking system. The robot would go to the station, dock itself to this support plate, grab the cables and connect them together. This docking procedure cannot be performed by the ROV operator because it requires very accurate displacements. An autopilot is then necessary so the ROV can dock automatically despite currents and other underwater hazards.

Some other tools include a positioning system needed to automate the docking procedure, a module to identify the cables underwater and a gripper to grasp the connector and connect it to the substation.

An additional study concerns the comparison of the models used to forecast wave energy with other renewable sources: wind and solar.

2. Theory

2.1 ROV hydrodynamics

When analyzing the motion of marine vehicles in 6 DOF it is convenient to define two coordinate frames, one is a moving coordinate frame B, which is fixed to the vehicle; it is called the body-fixed frame, its origin coinciding with the vehicle's center of gravity. The other one is an Earth-fixed coordinate frame and is called U, as shown in *Figure 6* below.

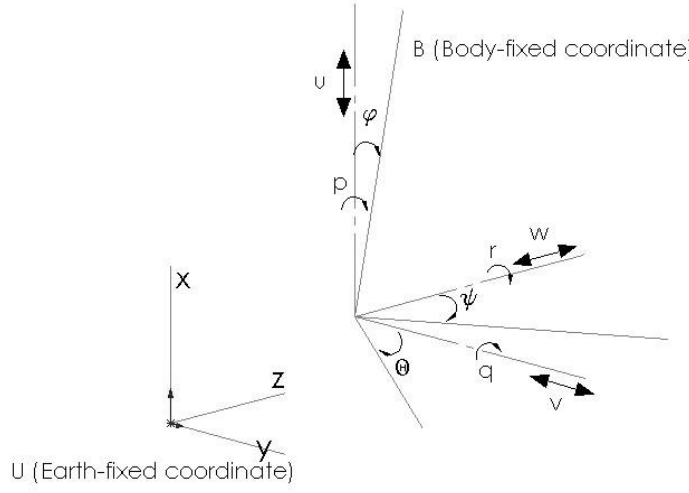

Figure 6. Body-fixed and Earth-fixed reference frames

We define the following notations:
$\eta = [x, y, z, \varphi, \theta, \psi]^T$ is the position of the origin of B and rotation of B expressed in U.
$\mu = [u, v, w, p, q, r]^T$ is the linear and angular velocity of the origin of B relative to U, expressed in B.

Table 2. *Notation used for marine vehicles*

Degree of Freedom	Translation and rotation	Linear and rotational velocities	Forces and moments
1- Motions in the x-direction (surge)	x	u	X
2- Motions in the y-direction (sway)	y	v	Y
3- Motions in the z-direction (heave)	z	w	Z
4- Rotations about the x-axis (roll)	φ	p	K
5- Rotations about the y-axis (pitch)	θ	q	M
6- Rotations about the z-axis (yaw)	ψ	r	N

The kinetics and kinematics of an underwater vehicle are well explained in [9], and will be summarized in the two following parts.

Kinematics

The vehicle's flight path relative to the Earth-fixed coordinate system is given by a velocity transformation:

$$\dot{\eta} = J_1(\eta)\mu \qquad (2.1.1)$$

where

$$J_1(\eta) = \begin{bmatrix} {}^U_B R(\phi,\theta,\psi) & 0 \\ 0 & T_\theta(\phi,\theta) \end{bmatrix}(\eta) = \begin{bmatrix} {}^U_B R(\phi,\theta,\psi) & 0 \\ 0 & T_\theta(\phi,\theta) \end{bmatrix},$$

with

$${}^U_B R(\phi,\theta,\psi) = \begin{bmatrix} c\theta c\psi & c\psi s\theta s\phi - s\psi c\phi & c\psi s\theta c\phi + s\psi s\phi \\ c\theta s\psi & s\psi s\theta s\phi + c\psi c\phi & s\psi s\theta c\phi - c\psi s\phi \\ -s\theta & c\theta s\phi & c\theta c\phi \end{bmatrix}$$

and

$$T_\theta(\phi,\theta) = \begin{bmatrix} 1 & s\phi t\theta & c\phi t\theta \\ 0 & c\phi & s\phi \\ 0 & \frac{s\phi}{c\theta} & \frac{c\phi}{c\theta} \end{bmatrix}, \theta \neq \pm 90^\circ,$$

$s\cdot = sin(\cdot), c\cdot = cos(\cdot), t\cdot = tan(\cdot).$

Kinetics

The dynamics equation can be expressed in the Body-fixed frame as:

$$M_{RB}\dot{\mu} + C_{RB}(\mu)\mu = \tau_{RB}, \qquad (2.1.2)$$

where M_{RB} is the rigid body inertia matrix, C_{RB} represents the Coriolis and centrifugal terms and τ_{RB} is a generalized vector of external forces and moments and can be decomposed as

$$\tau_{RB} = \tau + \tau_A + \tau_D + \tau_R + \tau_{dist}. \qquad (2.1.3)$$

- τ - as said above, vector of forces and torques due to thrusters/surfaces, which usually can be viewed as the control input,
- τ_A - The force and moment vector due to the hydrodynamic added mass,

$$\tau_A = -M_A\dot{\mu} - C_A(\mu)\mu \qquad (2.1.4)$$

- τ_D - Hydrodynamics terms due to lift, drag, skin friction, etc.

$$\tau_D = -D(\mu)\mu \qquad (2.1.5)$$

  Where $D(\mu)$ denotes the hydrodynamic damping matrix (positive definite).
- τ_R – Forces and torques due to buoyancy effects, also called restoring forces. Here, the restoring forces are not part of the model because we only consider displacements in the x-y plane for the docking procedure.
- τ_{dist} – Forces and torques due to disturbances. The disturbances, that take into account the currents, winds and waves, will be neglected in this paper: Although they are an important part of the equation they are very complex to model due to the high variability of their type, direction and speed. They are moreover difficult to measure with a system embedded in the vehicle.

The dynamics equation can now be written as:

$$(M_{RB} + M_A)\dot{\mu} + (C_{RB}(\mu) + C_A(\mu) + D(\mu))\mu = \tau \qquad (2.1.6)$$

It is necessary to know all those parameters and coefficients to calculate the ROV dynamic response to the command input. The added mass and drag coefficients $M_{A,}C_A, D$ are to be experimentally measured.

In the docking procedure we will for now neglect the depth control and therefore consider the ROV dynamics in 2 dimensions. Moreover in this thesis the ROV has three thrusters, one for vertical motion (which is not taken into

account here) and two for forward/backward, left/right movements, so the model becomes:

$$\begin{cases} \eta = [x, y, \psi]^T \\ \mu = [u, v, r]^T \\ \tau = [\tau_u, 0, \tau_r]^T \end{cases}$$

τ_u being the forward/backward thrust and τ_r being the torque for left/right motion.

$$M_A = \begin{bmatrix} X_{\dot{u}} & 0 & 0 \\ 0 & Y_{\dot{v}} & 0 \\ 0 & 0 & N_{\dot{r}} \end{bmatrix}, C_A = \begin{bmatrix} 0 & -Y_{\dot{v}} r & 0 \\ X_{\dot{u}} v & 0 & 0 \\ X_{\dot{u}} r & -Y_{\dot{v}} u & 0 \end{bmatrix}$$

where $X_{\dot{u}}, Y_{\dot{v}}$, and $N_{\dot{r}}$ are the added mass coefficients.

$$D(\mu) = \begin{bmatrix} d_u & 0 & 0 \\ 0 & d_v & 0 \\ 0 & 0 & d_r \end{bmatrix},$$

with:

$$\begin{cases} d_u = -X_u - X_{u|u|}|u| \\ d_v = -Y_v - Y_{v|v|}|v| \\ d_r = -N_r - N_{r|r|}|r| \end{cases}$$

where $X_u, X_{u|u|}, Y_v, Y_{v|v|}, N_r, N_{r|r|}$ are the drag coefficients.

Hence the final system of equations for the ROV model is:

$$\begin{cases} \frac{dx}{dt} = u\, cos(\psi) - v\, sin(\psi) \\ \frac{dy}{dt} = u\, sin(\psi) + v\, cos(\psi) \\ \frac{d\psi}{dt} = r \\ \frac{du}{dt} = \frac{1}{m_u}(m_v v r - d_u u + \tau_u) \\ \frac{dv}{dt} = \frac{1}{m_v}(-m_u u r - d_v v) \\ \frac{dr}{dt} = \frac{1}{m_r}(m_{uv} u v - d_r r + \tau_r) \end{cases} \qquad (2.1.7)$$

with $m_u = m - X_{\dot{u}}, m_v = m - Y_{\dot{v}}, m_r = I_z - N_{\dot{r}},\ m_{uv} = Y_{\dot{v}} - X_{\dot{u}}$.

2.2 Control Theory

Let's consider the following state space model:

$$\begin{cases} \dot{x} = Ax + Bu + Nv_1 \\ z = Mx \\ y = Cx + v_2 \end{cases} \qquad (2.2.1)$$

Where $\begin{bmatrix} v_1 \\ v_2 \end{bmatrix}$ is white noise with a Gaussian distribution and intensity $\begin{bmatrix} R_1 & R_{12} \\ R_{12} & R_2 \end{bmatrix}$ that corresponds to the disturbance sources, x is the state variable, z the controlled variable, y contains the measurements of the system, and u is the input.

We seek to minimize the controlled variable z and to keep the input u small. This can be translated in the minimization of the criterion:

$$V = \|z\|_{Q_1}^2 + \|u\|_{Q_2}^2 = E(z^T Q_1 z + u^T Q_2 u),$$

Where Q_1 and Q_2, the weighting matrices, are design parameters that are symmetric positive definite.

We consider here the case where the reference input is null.

The optimal controller for this system is the Linear Quadratic Gaussian control law $u = -L\hat{x}$ where $\hat{x}$ is obtained from the Kalman filter:

$$\dot{\hat{x}} = A\hat{x} + Bu + K(y - L\hat{x}) \qquad (2.2.2)$$

where K is the Kalman gain $K = PC^T R_2^{-1}$,

with P solving the continuous time Ricatti equation (CARE):

$$0 = AP + AP^{-1} + NR_1N^T - PC^T R_2^{-1} CP$$

and where L is the optimal state feedback gain $L = Q_2^{-1} B^T S$,

with S solving the CARE:

$$0 = A^T S + SA + M^T Q_1 M - SBQ_2^{-1} B^T S$$

More explanations can be found in [10]–[13].

2.3 Optical Positioning

Automatic docking is a very precise procedure that requires accurate positioning ([14]). Although acoustic systems such as sonars perform well for long distance measurements, they are not as efficient for short ranges. A solution for locating the ROV at a range from tens of cm to a few meters is to use an optical tool ([15]–[18]). In water, light can hardly travel more than hundreds

of meters because of scattering and absorption, see [17], [19]. The path of a light beam with attenuation can be described as:

$$I_t = I_0 e^{-a(\lambda)z} \qquad (2.3.1)$$

Where I_t is the transmitted irradiance, I_0 the original light irradiance, z the path length, and α(λ) the absorption coefficient of light, that depends on the wavelength λ. *Figure 7* presents a graph of this absorption coefficient depending on the wave length, coming from [20]. As can be seen in Figure 14, the wavelength that goes through water with the least absorption is 400-450 nm. This is why at sea, one sees everything in blue-green colors.

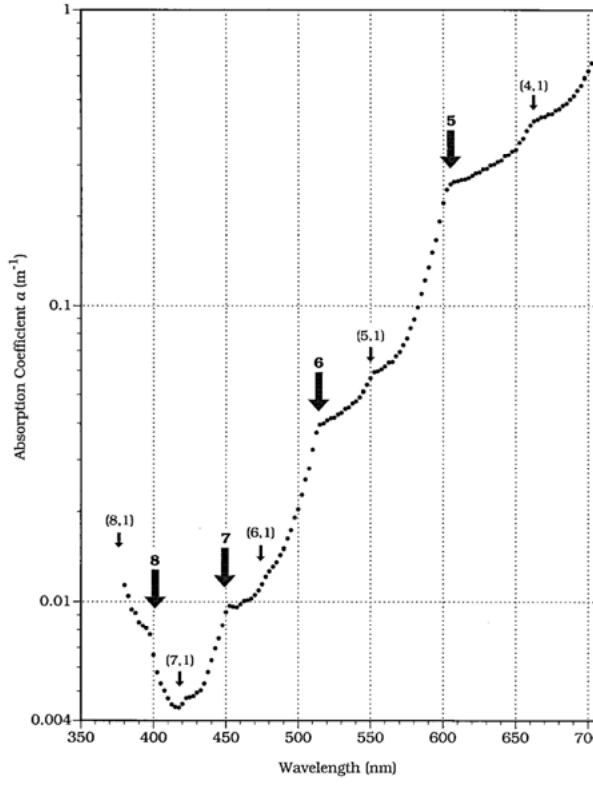

Figure 7. Absorption coefficient of visible light in pure water depending on the wavelength.

There are several ways to measure distances through visual recognition. Most of them use picture processing to identify particular areas, and determine their characteristics (Area, length, width, light intensity, color, etc.). With no need for very expensive hardware, picture processing can take advantage of the

three most important parameters for the device we are looking for: vision, accuracy and quite simple processing.

2.3.1 Laser positioning

The measurement method we chose to detect the docking platform is based on the apparent size of an object. The further away an object is, the smaller it looks, and conversely the closer it gets, the bigger it seems. Knowing that, if we know the exact length of an object we can determine how far it is just by measuring its apparent length. The object whose apparent size would be measured is a green laser, as its wavelength will not be as absorbed as quickly as others.
The system uses two parallel lasers as well as the ROV camera, and measures the distance between the centers of the dots as it is presented in *Figure 8*.

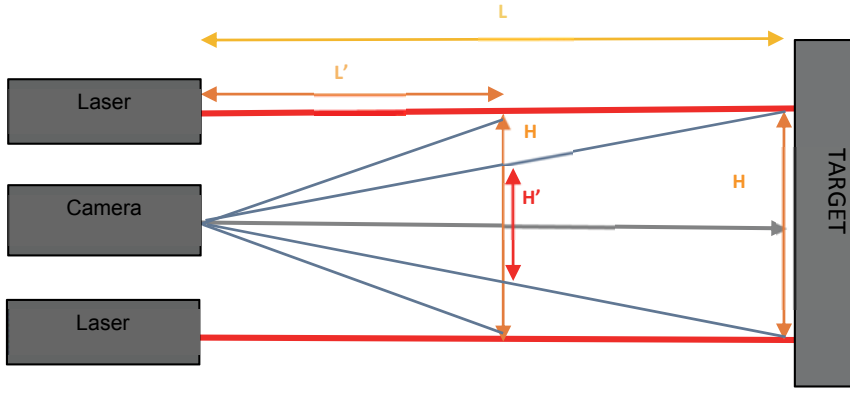

Figure 8. Scheme of the distance measurement device

From Thalès' theorem we have:

$$L = \frac{L' * H}{H'} \qquad (2.3.2)$$

The distance L' is a property of the camera. Therefore a calibration procedure is required in order for the equation to be solved. The distance H' is measured on the camera by counting the pixels between the two dots displayed.

Angle measurement:

So far, we assumed the target to be orthogonal to the camera axis, which means that on the target the distance between the laser dots is always the same.

In order to measure angles, the method is almost the same. Only here we measure two distances X_A and X_B instead of H', as it is shown on *Figure 9*.

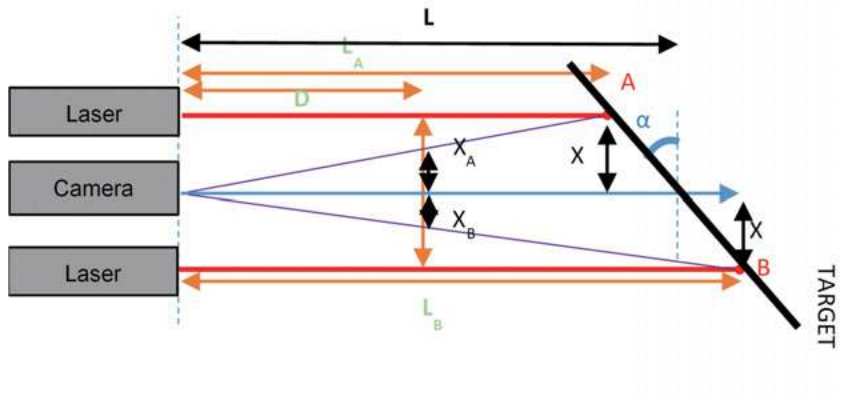

Figure 9. Scheme of the distance measurement device including angle measurement

From this figure above one can deduce:

$$L_A = \frac{D * X}{X_A}, L_B = \frac{D * X}{X_B} \quad (2.3.3)$$

$$L = \frac{L_A + L_B}{2} \quad (2.3.4)$$

$$\alpha = tan^{-1}\left(\frac{D}{2} * \frac{|X_A - X_B|}{X_A * X_B}\right), X_A, X_B \neq 0 \quad (2.3.5)$$

With α = 90° if $X_A = X_B = 0$.

2.3.2 Visual Odometry

Visual odometry is the process of determining the position and orientation of a robot by analyzing the associated camera images. In our case, we are using a single camera. By looking at the common points of two successive images, and determining where they are located in those images, one can compute the displacement performed by the robot to obtain this image transformation ([21]). *Figure 10* will give a visual idea of what odometry is.

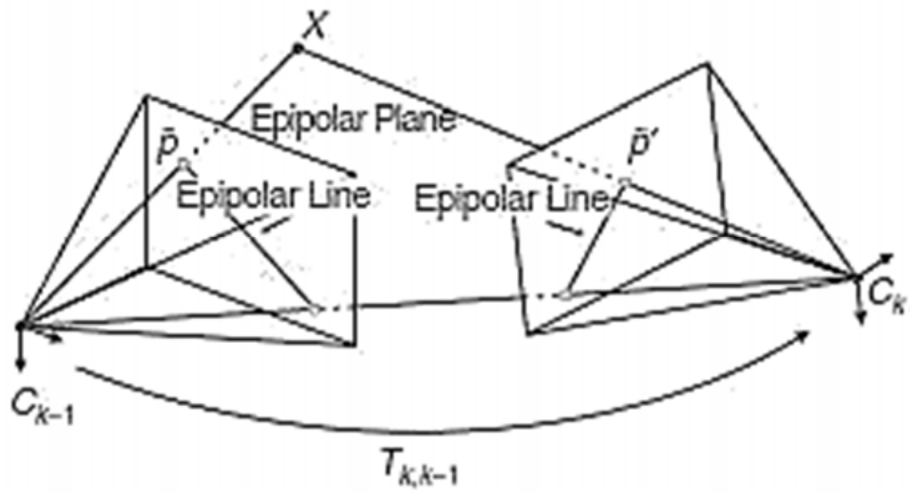

Figure 10. Presentation of visual odometry (from [21])

The algorithm follows these steps:
1. Capture image.
2. Detect key-points using the SURF algorithm (Speeded Up Robust features). If this is the first image, the algorithm store the key-points and stops there.
The SURF algorithm works as follows: An image is composed of multiple pixels associated to figures that correspond to each pixel's shade of grey. The key-points are detected if one or a small group of pixels has a remarkable (significantly different) intensity compared to the surrounding pixels. However noise could create local differences where there are in fact no real key points. Some filters are therefore used to cancel the noise and work on smoother data. In addition to that, different scales are taken into account in order to detect key points of different sizes in the same image.
3. Compare the key-points with the previous image key-points and find matches.
4. Determine the relative transformation between the two images. This is done using the RANSAC algorithm (Random Sample Consensus, also introduced in [22]) that works as follows: A random number (above the minimum required) of common points are selected, and the relative transformation between those points is computed. One then checks how much this transformation fits the other common points, with a predefined tolerance. If too many points do not belong to the margins of the transformation, one restart and choose a new number of key points. This method allows to remove the errors

in the image, for example when the SURF has detected a wrong key point or two common points that are in fact not common.
5. Store the current image as previous image.

2.4 Radio Frequency Identification

Radio Frequency Identification (RFID) has become an indispensable method for wireless identification and automated data capture. Those systems are used for contactless data exchange. The data is stored on an electronic data-carrying device: the transponder or tag. Transponders are available in different styles, depending on the used reading device. The reading device, called *interrogator* or *reader* is the data capture device.

Passive transponders have no inbuilt power supply. The required power needed for the communication with the reader is supplied without physical contact, but using electromagnetic fields instead.
A common distinction separates the systems into either Low Frequency (LF <135 kHz), High Frequency (HF at 13.56 MHz) or Ultra-High Frequency (UHF >2.5 GHz). The mentioned frequencies are the most popular ones, but variations cannot be ruled out.

LF RFID is based on the inductive coupling between the reader and the transponder, which is created by an alternating current sent into the reader's coil. At a sufficient distance, the magnetic field created by the current variations will induce a current in the transponder's coil. Switching a load resistor on and off at the transponder's antenna will then bring a change in the transponder's circuit impedance, and thus voltage changes at the reader's antenna. More explanation can be found in [23]. *Figure 11* presents a basic diagram of the RFID system.

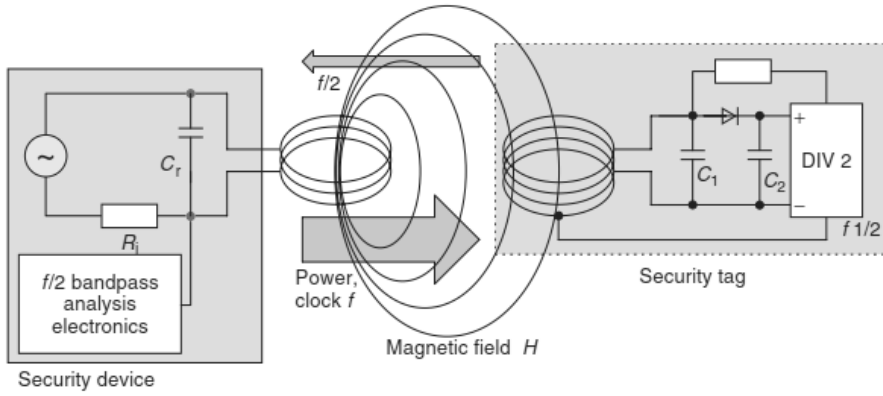

Figure 11. Basic circuit diagram of the radio frequency division procedure between the transponder (security tag) and the reader (security device) (from [23])

RFID in water

Water is a fairly unexplored environment for the use of radio frequency identification. The most important reason for this is probably that water is an inappropriate propagation medium for electromagnetic fields. The ability of electromagnetic waves to penetrate a conducting media is restricted by attenuation. As pure water can be seen as an isolator, water in its natural appearance can be a partial conductor due to the presence of salts and minerals (see [24]) The water attenuation coefficient, α, can be calculated as:

$$\propto = 0.0173 f\sigma \text{ dBm} \qquad (2.4.1)$$

Where f is the frequency in Hz, and σ is the conductivity of water expressed in S/m.

Below is a logarithmic graph of the attenuation coefficient as a function of the frequency, plotted for fresh water that has a conductivity of 0.05 S/m, and for salted water with a conductivity of 4 S/m.

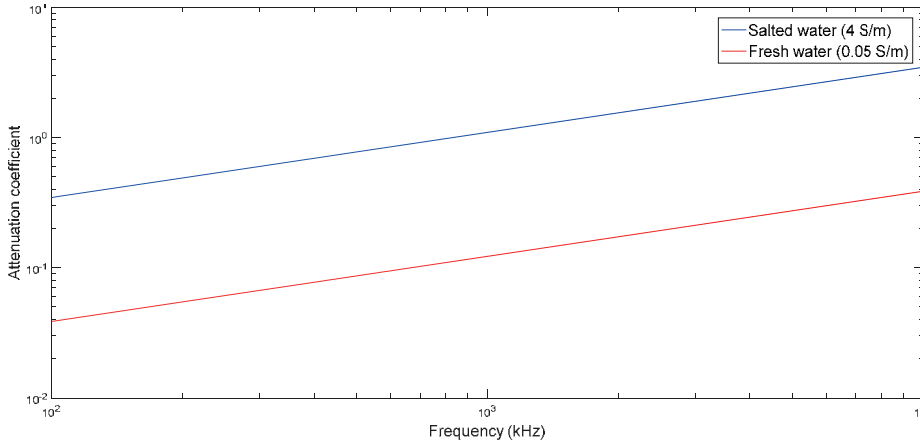

Figure 12. Water attenuation coefficient depending of the frequency for fresh and salted water

As it can be seen in *Figure 12*, the higher the frequency the larger the absorption of the radio wave. For this reason it is suitable to use low frequency readers in order to detect the cables under water. However too low frequencies cannot be used: first, they would require bigger antennas and consequently larger tags to be installed on the cables. Secondly, low frequencies are best suited for longer distances which is of no interest in this application. The ROV should be sufficiently close to the cable before identifying it, in order to not mix it up with other connectors in the vicinity.

3. Methods

3.1 OpenROV

OpenROV is a low cost open source ROV platform that makes it easy to implement tools, as a positioning or docking system, and to develop its control system. It is sold as a kit and only requires handy skills and soldering capabilities. The ROV can go 100 m deep. It has three thrusters, one for heave motion and two for surge and yaw, allowing a maximum speed of two knots. It is equipped with a HD Webcam, lights, two red lasers, a compass, and a pressure sensor for control of the depth and heading.

The power is supplied with help of batteries contained within the ROV (so no external power supply is required), and the electronics comprise a Beagle Bone Black computer together with a microcontroller board Arduino Mega that connect all the equipment and enable communication with the operator through Ethernet connection. The software is coded in node.js, a language that allows to use both JavaScript programming for the user interface and camera streaming, and C++ for the Arduino code.

The maximum thrust that each individual propeller can reach is 1 kg for horizontal forward motion. With two propellers the total forward thrust should theoretically be approximately 2 kg. It is also said that the four levels of power correspond to respectively 12%, 25%, 40%, and 75% of the total thrust in the OpenROV.

Below are two pictures of the OpenROV, prepared for sea trials (*Figure 13*) and in the laboratory (*Figure 14*).

Figure 13. OpenROV in Fiskebäcksskil

Figure 14. OpenROV in Ångström Laboratory at the test tank

3.2 Docking system for Remotely Operated Vehicle

As explained in the introduction, the docking procedure for an ROV requires very accurate displacements and hence an autopilot instead of a manual steering operation. This autopilot is first modelled in Matlab and will be implemented in the OpenROV in the future.

3.2.1 State space model of the autopilot for ROV

From section 2.1 and 2.2 we create the following state space model:

$$\begin{cases} \dot{x} = Ax + Bu \\ z = Mx \\ y = Cx + v_2 \end{cases}$$

where:

$x = \begin{bmatrix} \psi \\ u \\ v \\ r \end{bmatrix}$ is the state variable, $u = \begin{bmatrix} \tau_u \\ \tau_r \end{bmatrix}$ is the input sent to the thrusters, and corresponds to the forward thrust (τ_u) and rotational thrust around the z-axis (τ_r).

$y = z = \begin{bmatrix} u \\ \psi \end{bmatrix}$ is the speed and heading that are computed as the reference (Uref in the Simulink model),

$$A = \begin{bmatrix} 0 & 0 & 0 & 1 \\ 0 & -\frac{d_u}{m_u} & 0 & 0 \\ 0 & 0 & -\frac{d_v}{m_v} & \frac{m_u}{m_v} \\ 0 & 0 & \frac{m_{uv}}{m_r} & -\frac{d_r}{m_r} \end{bmatrix}, B = \begin{bmatrix} 0 & 0 \\ \frac{1}{m_u} & 0 \\ 0 & 0 \\ 0 & \frac{1}{m_r} \end{bmatrix}$$

with the coefficients $d_u, d_v, d_r, m_u, m_v, m_{uv}, m_r$ being defined in section 2.1.

$$C = \begin{bmatrix} 0 & 1 & 0 & 0 \\ 1 & 0 & 0 & 0 \end{bmatrix},$$

$$M = \begin{bmatrix} 0 & 1 & 0 & 0 \\ 1 & 0 & 0 & 0 \end{bmatrix}.$$

v_2 is a zero-mean white noise coming from the measurements disturbances.

3.2.2 Autopilot modelling

From this system, a model is created with Simulink and presented in *Figure 15*. The model contains three boxes: The path following unit, the ROV unit, and the positioning unit.

The path following unit takes as inputs the measured position when possible, the estimated position otherwise, and computes the reference input to guide the ROV on the desired path. The reference Uref is composed of the

speed and heading applied to the ROV, and is computed with help of a Proportional Integrator (PI) controller.

The ROV unit contains an inner-loop controller box that adapts the needed thrust for each of the propellers in order to reach the desired heading and speed. This thrust vector is then sent to the dynamics box, which is a model of the ROV dynamic response. This model has been presented in section 2.1. The output gives the position of the ROV and the actual state of the ROV. This state variable is composed of four components: the heading yaw, the x-directional speed u, y-directional speed v, and rotational speed around the z-axis r.

The positioning unit is a Kalman filter that estimates the ROV position, described in more detail in section 3.1.5. This filter is necessary in case of a sudden lack of sensory information, a software bug, or a delay in the response coming from the positioning system.

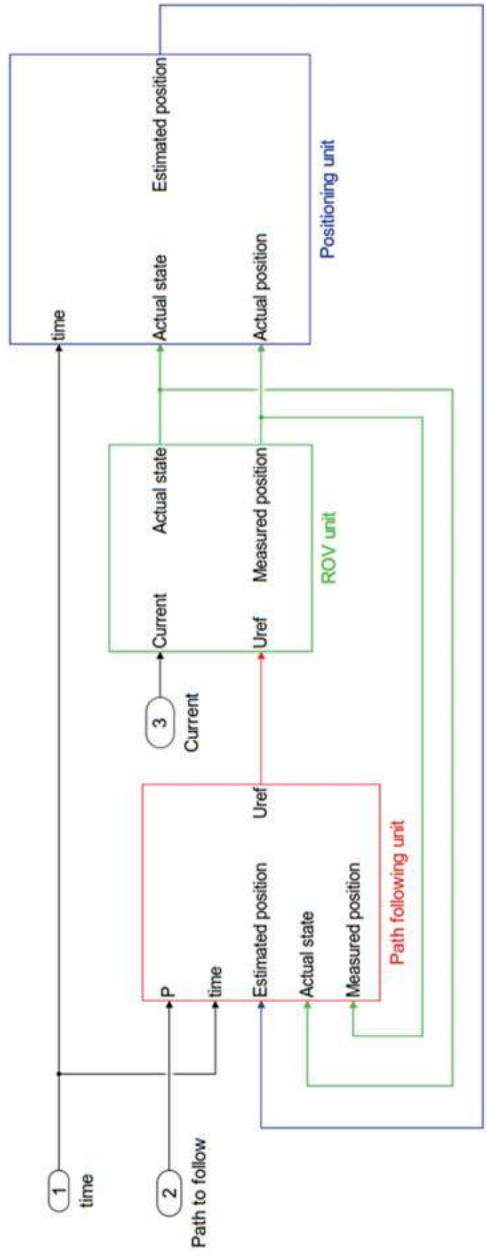

Figure 15. Simulink model of the autopilot for ROV.

3.2.3 Controllers

Two controllers are used in the model: One to compute the reference variables $Uref = \begin{bmatrix} u \\ \psi \end{bmatrix}$, depending on the present ROV motion state (measured or estimated) in order to follow the determined path; the other to compute the force and torque produced by the thrusters $u = \begin{bmatrix} \tau_u \\ \tau_r \end{bmatrix}$, depending on the reference $Uref$. The first controller is a PI controller that acts on the error between the estimated/measured and desired ROV position. It is described in [16][14]. The second controller is designed according to section 2.2 above. *Figure 16* and *Figure 17* present the two controllers designed in Simulink.

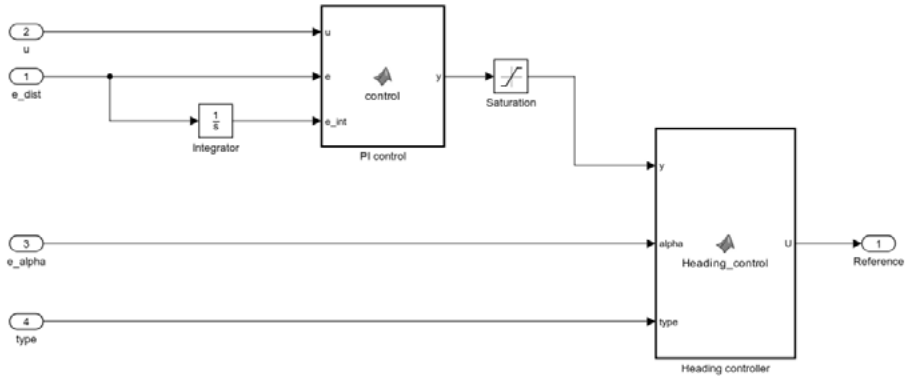

Figure 16. Path following controller

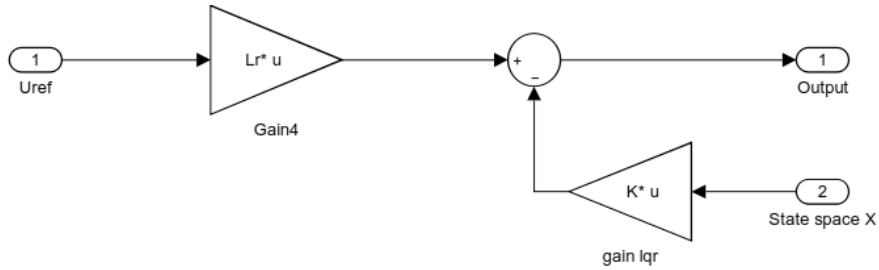

Figure 17. Inner-Loop controller

3.2.4 Thruster model

An accurate model of the thrusters is needed to get a dynamic response $\begin{bmatrix} \tau_u \\ \tau_r \end{bmatrix}$ from the command input. Indeed, if one gives a command to start the propellers, they will not react instantaneously but with a delay, oscillations and overshoot. This model is presented in *Figure 18*. The saturation boxes are here to limit the input thrust as the motors have limited power.

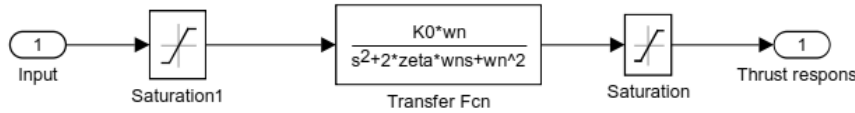

Figure 18. Simulink model of the ROV thrusters

The transfer function can be modeled as a second order system:

$$H_{th}(s) = \frac{K_{th}\omega_n^2}{s^2+2\zeta\omega_n s+\omega_n^2} \qquad 3.2.1$$

with K_{th} being the thruster gain, ω_n the natural frequency response in rad/s, and ζ the system's damping ratio.
Those parameters can be estimated with an identification method that correlate experimental data to the transfer function. The data contains the input commands, applied in 5 different steps, and the output thrust, measured by a strain gauge.

The experiments were done in the wave tank at Ångström Laboratory with the OpenROV. A Strain gauge (presented in *Figure 19* below) was glued on an acrylic plate, which was fixed on one side to a steel bar placed in the tank, and on the other side to the OpenROV. Incremental commands were sent to the robot, varying between 0, for no thrust, and 4, for 75% of maximal thrust. This input signal was timed and saved in a text file by Matlab. The ROV would pull on the acrylic plate, deforming the strain gauge. An amplifier would calculate the corresponding force and this response would also be recorded and saved in a text file.

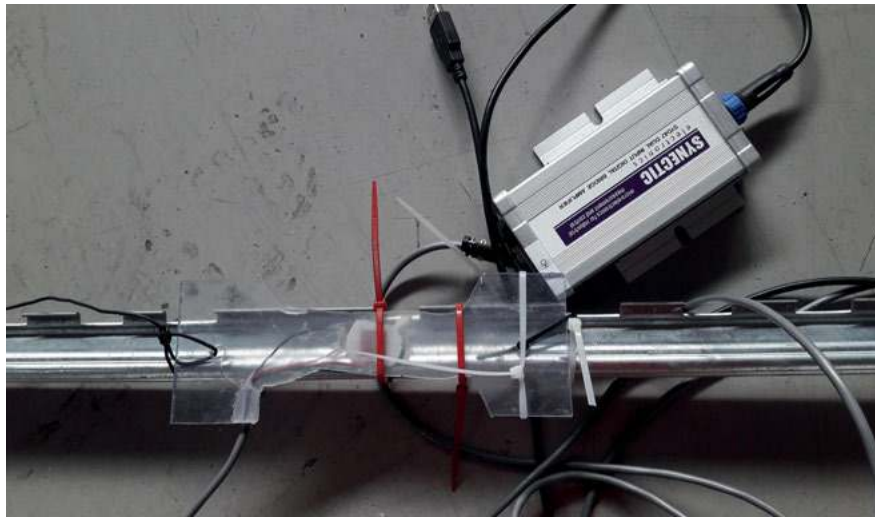

Figure 19. Strain gauge and amplifier used to measure the OpenROV thrust

3.2.5 Kalman filter

A Kalman filter is used in the model to estimate the position of the ROV. Indeed the sensors used to measure it in real time could be slow and/or noisy from time to time; a cut in the communication could also create a lack of data for the ROV. Therefore its position is always estimated and compared with measurements.

The Kalman filter works in two phases: The prediction phase gives the predicted state $\hat{x}_{k|k-1}$ depending on the previous state $\hat{x}_{k-1|k-1}$ and its covariance$P_{k-1|k-1}$. The update phase gives The value of the Kalman filter at the state k K_k depending on the state's covariance at state k-1, and the noise and its own covariance. It gives an update of the estimated state $\hat{x}_{k|k}$ and its covariance $P_{k|k}$.

3.3 ROV Positioning

3.3.1 Laser measurements in air

The positioning system was tested with red lasers in air. A plate representing the docking platform was placed at a certain distance to the ROV, with a certain angle to its trajectory line. The distance and angle were measured with the positioning tool and compared to the theoretical values. The experimental set up is presented below in *Figure 20*.

The program uses the library OpenCV (*Open Source Computer Vision*). OpenCV is a library of programming functions mainly aimed at real-time computer vision. With the help of this library, it is possible for the program to capture a snapshot from the camera, find the two laser dots, and measure their relative distance on the camera picture. It then calculates the real distance and angle between the ROV and the plate.

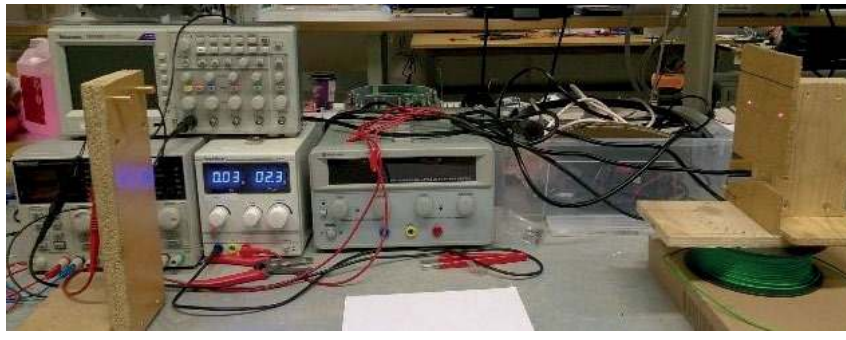

Figure 20. Experimental setup for laser measurements in air

3.3.2 Visual odometry

The program uses OpenCV 3.1, as the laser positioning system, and several additional modules that must be installed on the computer. The first phase is a calibration program that is required in order to obtain the intrinsic parameters of the camera. With the help of a chessboard we get the focal length, the distortion factors, and the main points of the camera. Then the data stream is captured and several key points are detected. By comparing two successive images, a matrix is created with all the matches from one image to another. We use this matrix to find the transformation between two successive positions of the ROV and store the results in a file.

3.4 Gripper for cable connection

Designing a gripper for cable connection is a rather big challenge and the main tasks are the following:

- Keeping the connectors aligned
- Pushing/Pulling with a sufficient force to connect/disconnect the 2 parts
- Pushing softly the connectors in order to not break them, i.e. knowing when the connection is completed
- Holding the connector so it does not slip while being mated

Solving these issues is possible with the help of several sensors placed on the gripper and a very good control system for accurate displacement.
Some first trials were made to design a gripper with two claws already aligned, as can be seen in *Figure 21* and *Figure 21*.

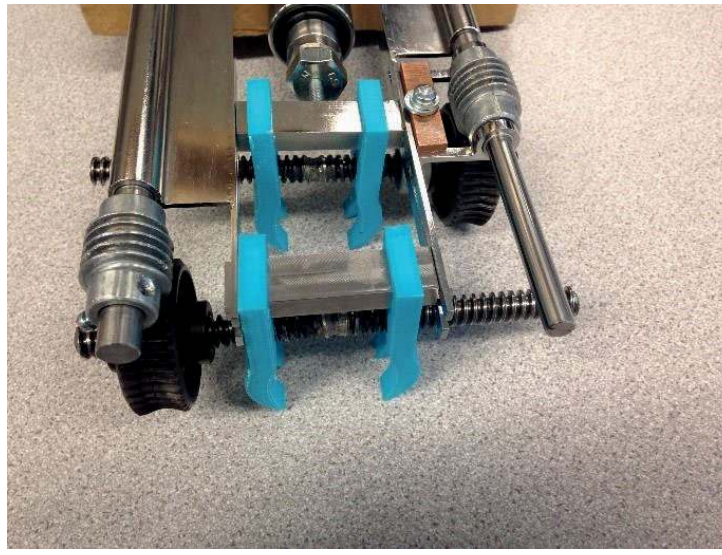

Figure 21: Gripper prototype A for cable connection

Figure 22. Gripper prototype B for cable connection

The motors are sealed in a box with a magnetic transmission for the first design, and a regular shaft sealed with help of two watertight bearings in the other design, see figure 22. In both case the actuator was purchased already sealed.

3.5 Underwater cable detection

As mentioned before the RFID reader was chosen to operate at a frequency of 125 kHz. The device is called *ID-70 LF reader* and comes from the company *ID-Innovations*. It was purchased because its features are compatible with our requirements: It works in the long frequency (LF) range and uses a kind of tag named *EM4102* that is a very common transponder type in RFID systems. At least 90% of the RFID systems currently sold are inductively coupled systems with EM4102 transponder ([23], [25]).

3.5.1 Control unit, power and communication

It was decided to use an Arduino microcontroller UNO as the host system because the Arduino is low cost and simple to use. The choice for output format was Wiegand26 because it can be easily imported in an Arduino microcontroller with help of a library. A LCD screen was added in order to display the ID number of the detected tag. A 9 V battery would supply the Arduino, as a 12 V Lead-Acid battery would power the ID-70 reader. *Figure 23* presents the control unit and communication between the reader and the LCD screen that.

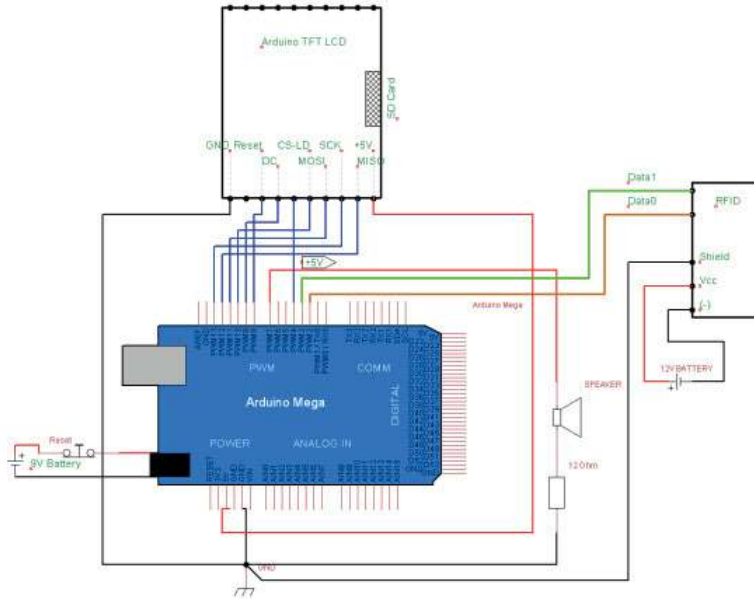

Figure 23. Circuit diagram of the control unit for the ID-70 reader.

There was no ROV available at the division for Electricity at the time of the project, so it was decided to design a system that uses its own power and data cable between the reader and the control unit. By doing this the ID tool is independent from the used hardware and interfaces of the ROV. This also implicates some difficulties for the use of the tool because there will be two cables in the water, one for the ROV and one for the identification tool. But this issue can be improved when the use of an ROV is enforced in the Lysekil Project.

3.5.2 Experiments

Tank experiments were done at Ångström Laboratory in order to measure the detection range of the reader. The reader was placed in water and moved until the tag was detected. The detection distance was then measured; it is the distance *d* on the *Figure 25*. Different transponders were used; *Figure 24* shows the four EM4201 transponders used and a 5 cents Euro coin for size comparison. To investigate the impact of transponder orientation on the reading range, four different measurements were done. Either, reader and transponder were placed in the same axis, which is described by the symbol ∥, or reader and transponder were placed in different orientations with a 90° angle between each other, which is labeled with ⊢, as it is seen in *Figure 25*. The experiments were done in a small pool (1*0.5 m²) filled with salted water with a conductivity of 4 S/m.

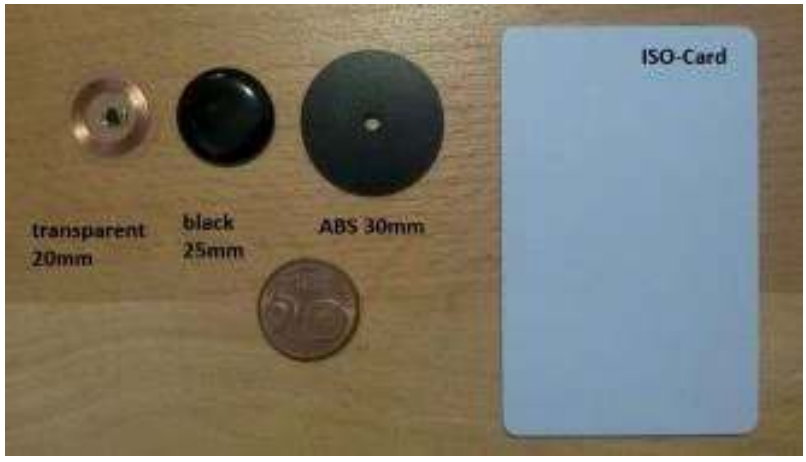

Figure 24. Transponders used for the cable detection

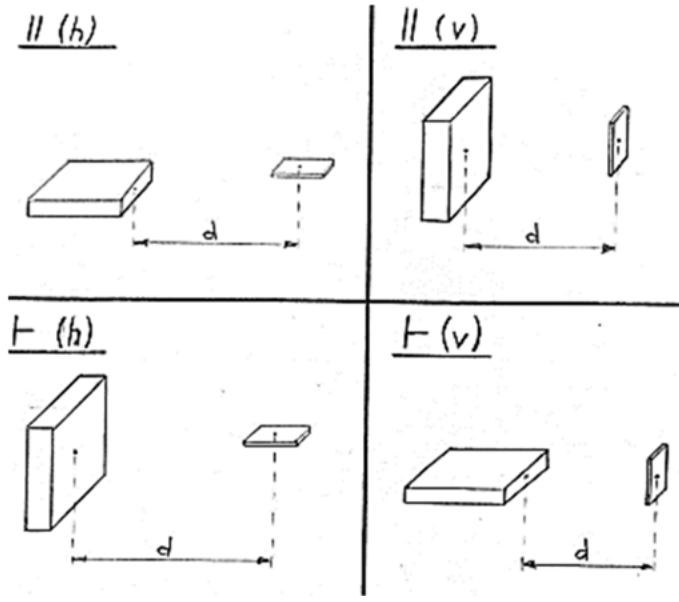

Figure 25. Different measurements done to compare the ways of detection

3.6 Forecasting wave energy among other renewable sources

Forecasting is a major issue in the integration of variable renewable source into the power system. One significant factor is the time horizon that varies significantly between solar, wind, and wave energy. While the forecasting time horizon varies from about 30 s to 10 days for solar energy, it is between 30 min and a few days for wave energy. Forecasts between sub-seconds and minutes can be used in the active control of the turbines in wind or wave energy, while several days forecasts are necessary to plan maintenance of the farms and the electrical grid.

Forecasting models can be broadly categorized into statistical and physical models. Statistical models apply statistical methods on existing time-series of the resource, and do not involve any physical modelling of the resource. In contrast, physical models include a physical modelling of the atmosphere, based on different types of atmospheric data. Hybrids of physical and statistical models are also common, not least in operating commercial forecasting software, whether for wind, wave or solar energy.

3.6.1 Forecasting accuracy metrics

To be able to compare the forecasting accuracy of different methods, a common accuracy metric is needed. However these metrics used differ between the studied renewable energy resources. This poses a challenge in comparing the accuracy of the forecasts on different spatial and temporal domains.

Concerning wave energy, the metrics and units used for forecasting are very disparate. The calculated errors refer to many parameters, such as wave height, time period, energy power output, and a variation of different metrics are used, such as MAE, RMSE, correlation, bias, etc. It is common among wind and solar energy to compare forecasting skills with help of a reference model, but in wave power this model is seldom used which makes comparisons difficult within wave forecasting models.

3.6.2 Forecasting models

The accuracy of forecasting models depends on the time horizon and the spatial resolution, and different methods are suitable for different temporal and spatial domains. A broad overview of recommended forecasting methods for the solar, wind and wave resources, as a function of temporal and spatial resolution, is shown in Fig. 26. The figure shows that physical models are generally preferred over statistical models on longer time horizons and lower spatial resolutions. The figure includes the use of a persistence model, or naïve predictor, which is a reference model where the energy of the resource is predicted to remain unchanged over the forecasted period.

Among the statistical models, there are more traditional approaches such as autoregressive analysis (AR), as well as more recently developed models. The latter include wavelet transforms and learning models such as k-nearest neighbor (k-NN) or artificial neural networks (ANN), sometimes combined with genetic algorithms (GA). All those models are used in all the renewable energies that need forecasting, such as wind, wave or solar energy.

The physical models use different data inputs depending on the resource and are specific to each renewable energy. Concerning waves the state-of-the-art formulations of the processes of wave generation, dissipation, and wave-wave interactions in phase averaged models are presently third generation, e.g., WAM [26], SWAN [27] , MIKE-21 [28], Mar3G [29]. A more detailed list of wave models operated by various national Meteorological Services is given in [30].

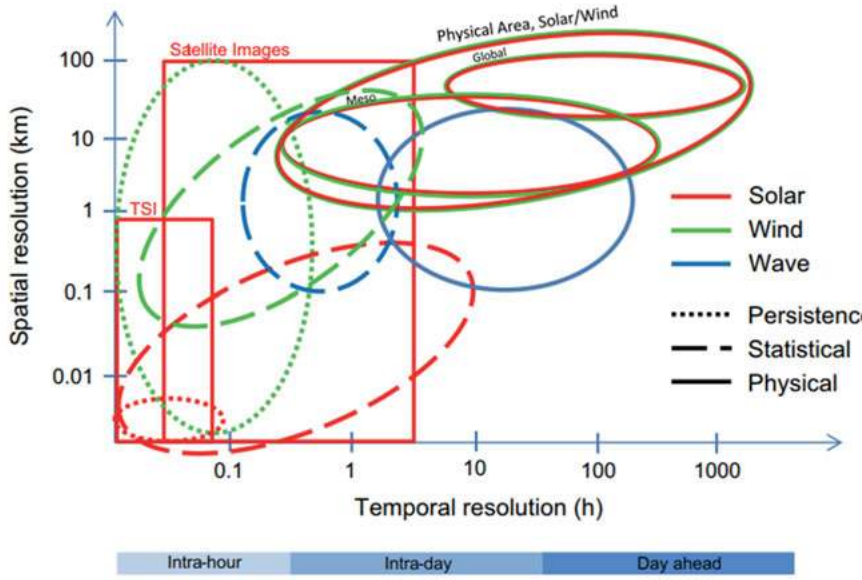

Figure 26. Comparison of forecasting methods between wind, solar, and wave energy, depending on temporal and special resolution.

4. Results and Discussion

4.1 Model of thrusters

4.1.1 Calibration and experiment

The calibration was done with help of weights of 0.1, 0.5, 1.0, and 1.75 kg, presented in Figure 27 below. The weights were hanging and making the sensor bend.
The linear function associated to the calibration is the following:

$$y=kx+m, \qquad 4.1.1$$

with $\begin{cases} k = 3.3533e-05 \\ m = -0.18437 \end{cases}$,
where x is the output signal from the strain gauge amplifier. The signal has a 24 bit resolution and the amplifier has a sampling rate of 470 reading per second, with an output rang of +/-500000 counts.

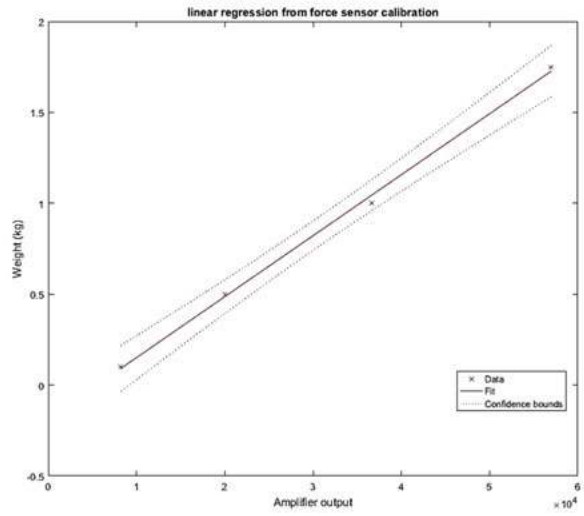

Figure 27. Linear regression for the force sensor calibration

The Root Mean Square Error (RMSE) is 0.0374. We can consequently trust the signal given by the sensor for a weight in the range of 100 g - 2 kg. Each time the weight is dropped the line slacks before reaching the right position. This is due to the elasticity of the line used, which makes the system act like an oscillating spring.
We observe the same oscillating effect in the experiment from the OpenROV tank trial, presented in Figure 9. On this graph one can see the response of the thrusters to the successive power levels given as command inputs. The signal gets noisier as the power increases. One possible explanation for this is that the higher thrust from the propellers induces turbulent water currents in the small tank. This turbulence makes the sensors move and vibrate, which causes the noise. Another cause to the observed noise is the inaccurate perpendicularity between the thrust direction and the sensor axis. Consequently the strain gage deforms in the other directions, inducing disturbances in the output voltage variations.

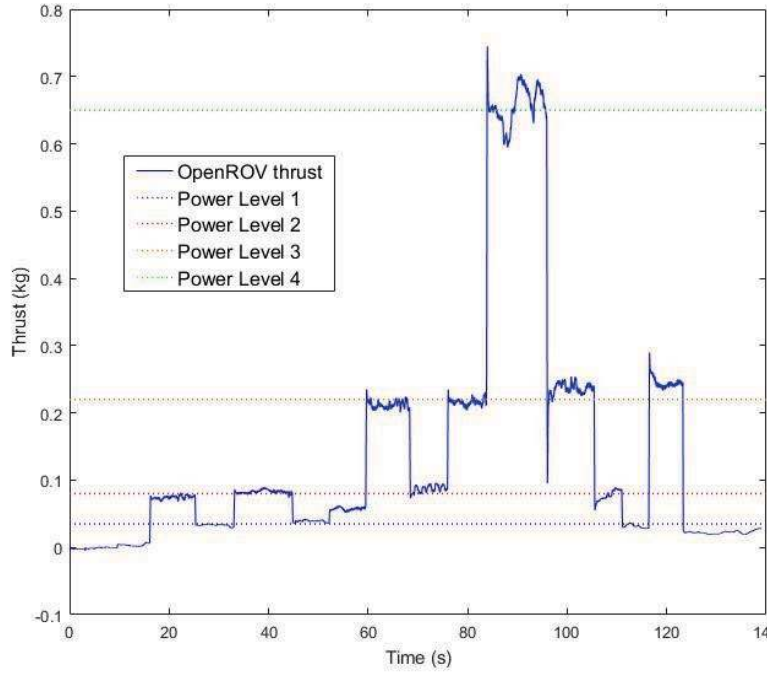

Figure 28. OpenROV thrust response to 4 power level commands

From [31], [32] one should expect power levels corresponding to respectively 12%, 25%, 40%, and 75% of a maximum thrust of 2 kg. On the graph, however, these values are not reached at all. If we take the level 4 as 75% as it was planned, then the maximal thrust becomes 0.91 kg, and the levels 1 to 3 correspond respectively to 7%, 12%, and 27%.

The difference between the theoretical and experimental maximum thrust can be explained by several reasons. First, 1 kg per propeller is given for the propeller alone, and should normally decrease when the propeller is attached to the ROV. Secondly, it is likely that some losses occur in the electronics, and the current sent to the motor is then lower than it should be. Another reason is the fact that the two propellers spin in opposite directions, so when one is in the forward mode, the other is in the backward mode, which is weaker than the forward one. So the total thrust should be less than 2 kg. Finally, the size of the tank and the measurement system disturb the flow and hence the experiment itself. The losses are in great part caused by those disturbances and explain the difference between the theoretical and measured percentages for the four power levels.

4.1.2 OpenROV thrusters model

After filtering the signal with a low pass filter, we can identify a second order transfer function that will model the thrust response to the four step inputs corresponding to the four power levels.
Figure 29 below presents a zoom of the filtered signal for the different power level steps: 3 to 4, 4 to 3, 2 to 3, 3 to 2, 1 to 2, and 2 to 1.

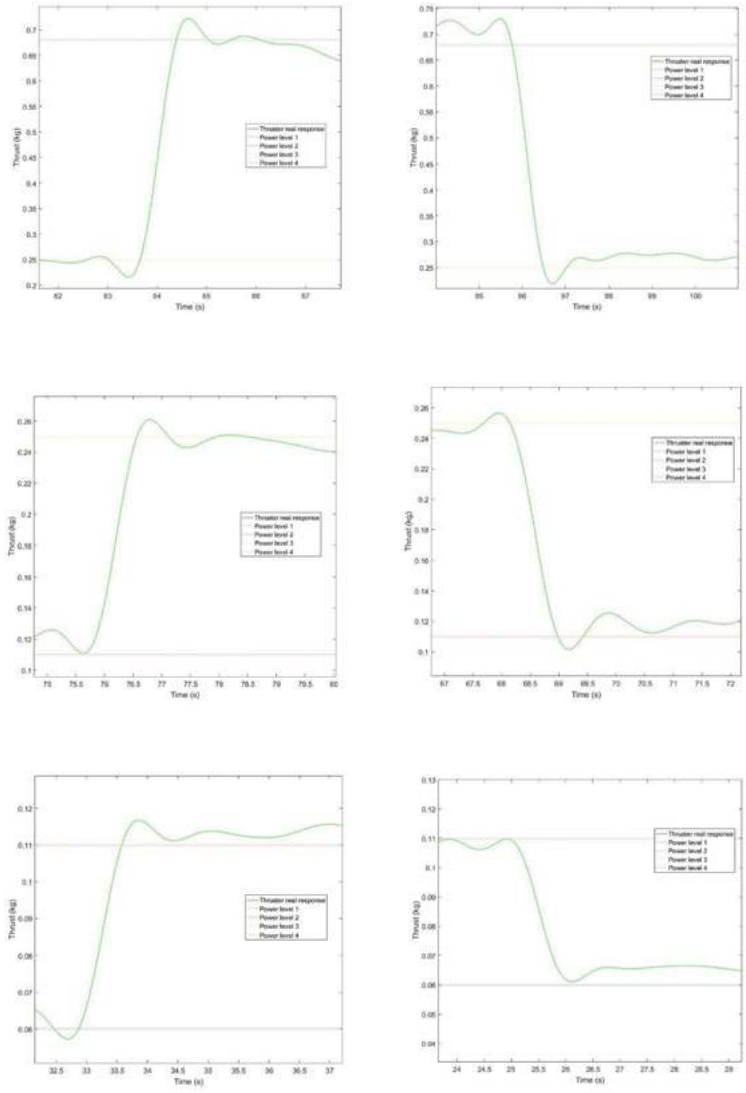

Figure 29. Thrusters step response for the four power levels

After filtering the signal with a low pass filter, we can identify a second order transfer function that will model the thrust response to the four step inputs corresponding to the four power levels.

From those filtered signals, a model is designed that approximates in average the response of the thrusters. As described in 3.2.4, the model is a second order transfer function, and the identification gives the following parameters:

$$\begin{cases} K_{th} = 1 \\ \omega_{\mathrm{n}} = 3{,}62\,\dfrac{rad}{s} \\ \zeta = 0{,}4 \end{cases}$$

The graph in *Figure 30* superimposes the two responses: the one from the experiment, after being filtered, and the one simulated from the model.

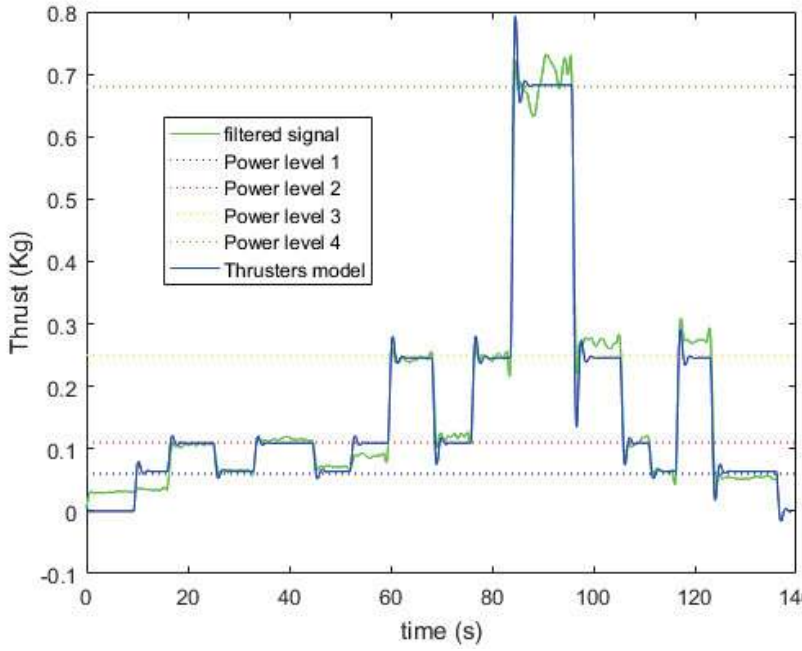

Figure 30. Model of thrusters compared with the filtered signal from the experiment

The damping ratio is adjusted in order not to take into account the effect of elasticity in the measurement line holding the OpenROV. From the calibration phase this elasticity is estimated to be 6% of the overall damping.

4.2 Positioning tool

4.2.1 Laser measurements

The results for the distance measurements are presented in *Figure 31* that shows the evolution of the error with the increasing distance between the lasers and the docking platform. This error slightly increases from almost 0% for 51 cm to around 5% for a distance of 311 cm.

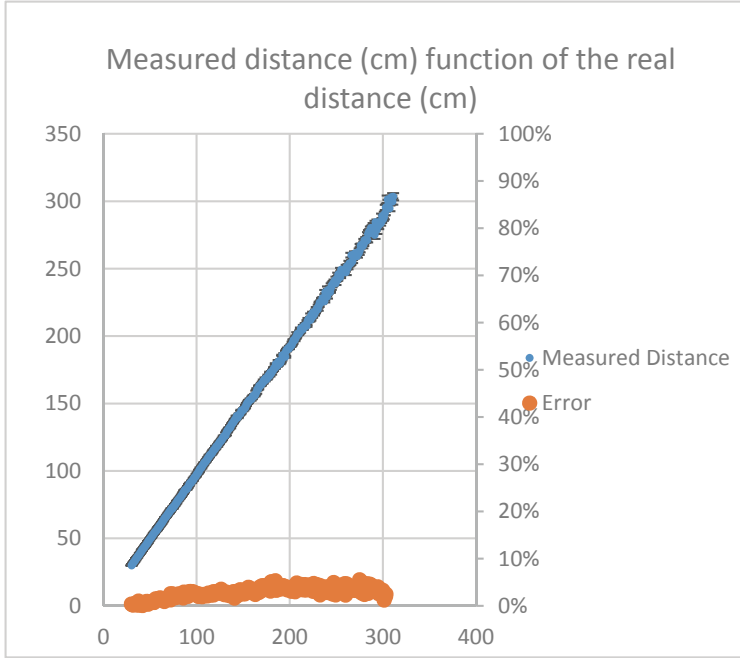

Figure 31. Measured distance and error function of the real distance

The measurements of the angle can be seen in *Figure 32***Fel! Hittar inte referenskälla.** with an average error of 6% at 55 cm distance, and *Figure 33* with an error of around 20% at a distance of 261 cm.

Those results are reasonable when the plate is perpendicular to the ROV's trajectory. Indeed, the error starts from 5% for large distances (around 3 m), and then decreases as the vehicle gets closer to the platform, to a maximum 3% for a distance of 50 cm, which means around 1.5 cm accuracy. This error is acceptable if the docking station is equipped with a mechanical guidance system. However, the angle measurements do not give very satisfying results.

Nevertheless it is possible to mediate this issue by adding a third laser to the positioning system. The accuracy would increase significantly without complicating much the program and the tool in terms of electronics and space.

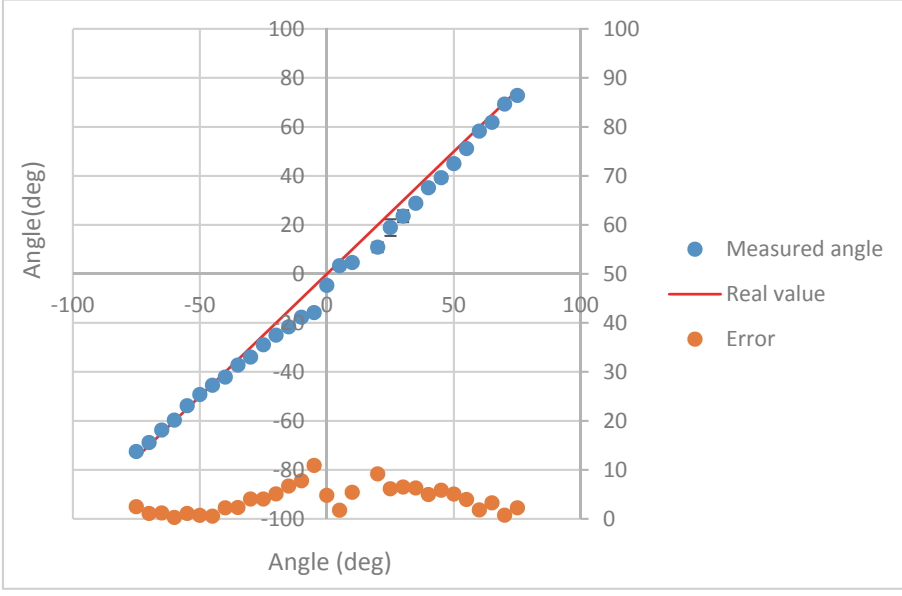

Figure 32. Measured angle compared to real angle at 55 cm distance

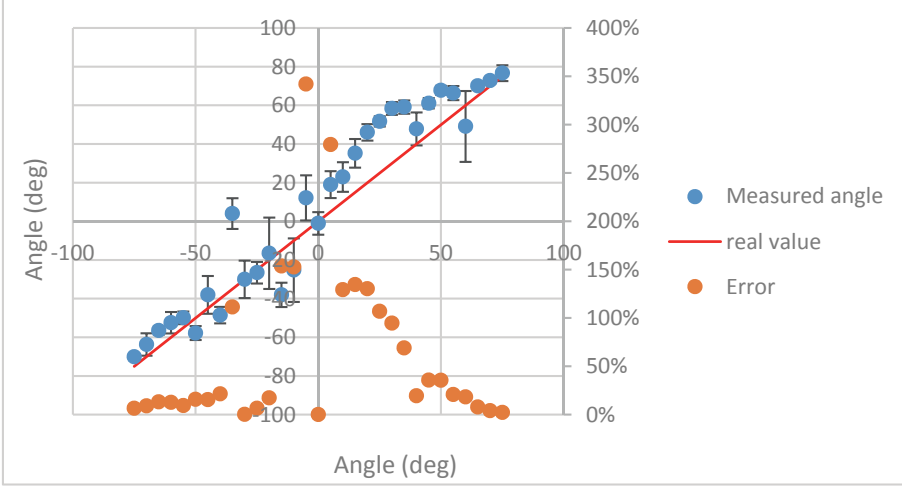

Figure 33. Measured angle and error comparde to real angle at 261 cm distance

4.3 Gripper for cable connection

The first gripper prototype was made to fit exactly the Lysekil substation design. The transmission for the gripping part was done by a worm gear, which causes non negligible losses. A very powerful motor was then necessary to perform a good grip between the claw and the connector, which increased its size and weight and made it soles than ideal. Therefore another design was created, that is more robust. The new guiding system allows a better alignment between the two connectors.
The sealing of the motor was another issue. The first design used a magnetic transmission, but the losses were significant. The second one used waterproof bearings, which gave much better results.

4.4 Underwater cable detection

Table 3 presents the results of the experiment for cable detection, made in a tank at Ångström Laboratory. It appears that the ISO Card, which has the biggest antenna, was detected at the longest distance, and the detection range then decreased as the size of the tag gets smaller. The results of the experiments were consequently as expected.

Table 3. *Mean and standard deviation in cm of the detection range between the reader ID-70 and four different tags in four different positions*

Transponder	∥ (v)	∥ (h)	⊢ (h)	⊢ (v)
ISO Card	52.33 ± 0.47	31.50 ± 0	22.67 ± 0.24	18.33 ± 0.24
ABS 30 mm	44.67 ± 0.24	25.67 ± 0.24	22.00 ± 0.41	13.17 ± 0.47
Black 25 mm	39.0 ± 0	23.33 ± 0.24	20.67 ± 0.24	12.67 ± 0.24
Transparent 20 mm	36.5 ± 0	21.33 ± 0.24	19.17 ± 0.24	10 ± 0

The reading range of 0.5 m seems acceptable for an ROV to detect a connector. However the squared geometry of the ISO Card makes it useless to attach it to any cable. The ABS tag, in the contrary, with its hole in the middle, can be easily fixed with a strap.

A test in Lysekil using those tags was made, with the help of a small ROV called VideoRay. The purpose of the test was to verify if the connector would be detected at 25 m depth, and the experiment was successful. At a depth of 25 m it was not possible to measure the range of detection because the position of neither the connector nor the ROV are known. The setup is presented in *Figure 34*.

Figure 34. Test in Lysekil with the VideoRay ROV and the RFID system

The identification tool is low cost and very easy to implement. A simple database enables the identification of each connector and its position at the substation. It could have other uses, for example to detect WECs in the water. For now each of them is different and far from each other, and therefore recognizable. But in the future it would be necessary to have tags in order to differentiate them, especially when they are close to each other.

4.5 Comparison of forecasting skills for wave, wind, and solar energy

In order to compare forecasting skills for the different energy sources, the persistence model was used as a reference and the skill score was calculated based on the metrics used in the respective studies, as indicated in Table 4. *Figure 35* compares forecasting skills for different models proposed in the literature. The details for the models represented by each curve are listed in Table 4. For each curve, the x-axis represents the time-horizon, and the y-axis represents the forecasting skill. The metric is RMSE for wind and solar resources, MAE for wave resource.

Table 4. *Details for the models compared in Figure 35.*

Nr	Re-source	Method used	Site	Metrics	Unit
1	Solar	Physical: Satellite Images (SI) and NWP, (NDFD)	6 sites across the US	RMSE	W/m^2
2	Solar	Physical: NWP, (WRF)	Andalusia, Spain	RMSE	W/m^2
3	Solar	Statistical: ANN	Ajaccio, France	RMSE	J /m^2
4	Solar	Statistical: ANN+GA	California	RMSE	W
5	Solar	Hybrid ANN+SI+lagged GHI	Spain	RMSE	W/m^2
6	Wave	Physical: SWAN Statistical: Spectral model	Four different sites in Atlantic and one in Pacific ocean	MAE	m (wave height)
7	Wave	Statistical: mix of neural network and regressions. Two different time horizons analyzed: short-term and long-term	Four different locations in the Pacific ocean	MAPE (mean absolute percent error)	W
8	Wind	Statistical: Markov-Switching Autoregressive model	Two different offshore parks in Denmark	RMSE	W
9	Wind	Physical: Combined physical and statistical (Fuzzy-NN)	11 wind farms in Ireland	RMSE	W
10	Wind	Statistical: ARIMA-GARCH	64 wind farms in Ireland	RMSE	W

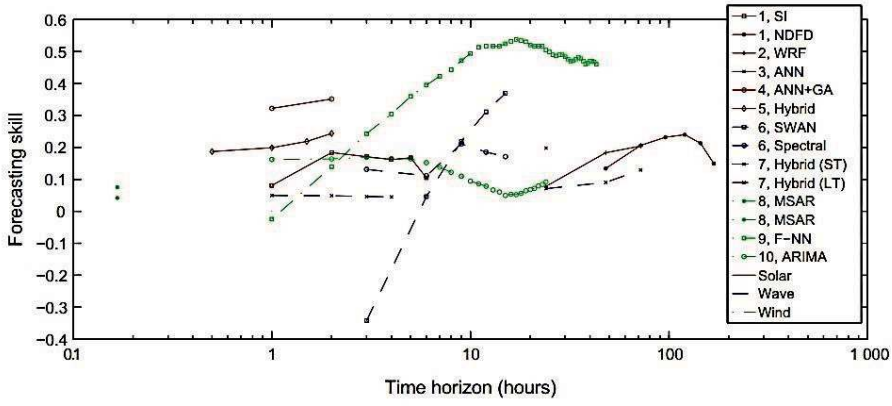

Figure 35. Comparison of forecasting skills for different models in solar, wave, and wind energy

The values for the forecasting skill get close to one as the method used gets better compared to the persistence model. Negative values mean that the persistence model is better than the evaluated method. For the same resource, one can compare different methods by looking at the forecasting skill values: the higher they are, the better the method is. However this does not say if the method is good or not.

In *Figure 35* we can observe that overall for solar, wind and wave, the forecasting skill for statistical models has a tendency to be higher than for physical models for the short time horizons and lower for long time horizons. This supports the statement asserting that statistical models outperform physical models for short time horizons, and the opposite for long time horizons.

However, the conclusions are limited by the use of persistence models which are not the same for all the sources in this figure. This causes problems when the renewable energy resources are compared to one another. The strength of the persistence models is that they provide a way to compare studies that have used different error metrics, although it has to be kept in mind that different metrics can still give different skill scores. However, when one persistence model is needed for e.g. solar and a different one for wind, then the inherent differences between the persistence models themselves introduce uncertainties into the study that ultimately makes it difficult to compare the variability of one resource to another. This leads us to question the use of persistence models if more than one is needed for a study.

5. Conclusion

Using an Observation Class ROV to perform cable connections is a big challenge, but we show here that it can be realized by the use of suitable tools and modules. One of the requirements is the design of a good positioning system. The use of green lasers is a low cost and simple solution, although a system with three lasers will give more accurate results than with two, especially for angular measurements. It is also interesting to use odometry in combination with the lasers in order to improve the relative positioning.

Designing an autopilot requires the modelling of different sub systems, as the thrusters, the hydrodynamic behavior of the ROV, controllers and estimators. Those models give already good results, but can always be improved. Knowing the hydrodynamic coefficients of the ROV will allow the model, and its different subsystems that are the following path, the ROV response, and the positioning unit, to be tested.

Concerning the gripper, it still requires significant improvement. The time needed to develop a proper gripper has been found to be too much for this project and will thus be excluded from it.

The RFID module is a good tool for any identification underwater. It could have other uses than cable detection and its light weight, low price, easy implementation, make it interesting for any Observation Class ROV.

The review on forecasting skills between solar, wave, and wind energy gave a good insight on the different models used for forecasting each resource. It should be possible to extend methods mainly used in one field to the other ones, and to synchronize data collection and modelling. For example, the same general statistical models for plant correlation and overall aggregated variability can be used for all sources.

6. Future Work

The next step will consist in developing the positioning system that will allow the OpenROV to detect its environment and displacements underwater. This tool will also enable the estimation of the OpenROV hydrodynamics coefficients. Once this is completed it will be possible to finish designing and implement the autopilot for the OpenROV.

If there is time left it would be very interesting to build a bigger and stronger ROV that could actually grab a cable on the seabed. A good solution would be to have those two ROVs, one “big and stupid” that will do the work, following the orders of the “small and smart” ROV, the latter being equipeded with the positioning system and the autopilot. One such big ROV is actually being built at Ångström Laboratory and fits the requirements to operate at Lysekil.

7. Summary of Papers

Paper I

Automation of subsea connection for clusters of wave energy converters

The paper reviews the different connectors used in ORE, the different types of ROVs, and describes the connection procedure at the Lysekil substation. In a second part it presents the first tank trials that were conducted to perform a connection underwater with an OCROV. The results of the tests allow to say that connecting cables with an ROV is not a trivial task, even in a tank with no currents and good visibility, and requires a docking system as well as an autopilot, and a gripper that will help and guide the connection.

The author did not take part in the trials, but summarized the conclusions of the tests, did both reviews and wrote the paper.

Paper II

Wave Energy Research at Uppsala University and the Lysekil Research Site, Sweden: A Status Update

The paper gives a status update of the Lysekil Project. After introducing the project, the test site, and the wave power concept, it describes the evolution of the different WECs and their performances, the different types of buoys studied and tested. The substation and measuring station updates are presented. In a 5th part the ROV project is introduced as well as a RFID (Radio Frequency Identification) tool to recognize the connectors underwater and their position at the substation. Some studies are presented, concerning the modelling of wave power farms, survivability in extreme conditions, as well as environment. Finally some updates on grid connection are presented.

The author participated in writing the part on ROV trials and presenting the RFID tool.

Paper III

Optical System for Underwater Positioning of Observation Class Remotely Operated Vehicle

The paper presents the docking system for ROV and need for a positioning tool. It reviews different positioning devices and describes the optical one, made of two lasers. Some tests were done with accurate results when the lasers are perpendicular to the docking platform (error < 5%). For angle measurement the error is higher but this issue can be solved by including a third laser in the system. The discussion part describes and measures the errors coming from a non-parallelism between the two lasers, or from the casing in which the lasers will be enclosed.

The author performed most of the work in this paper.

Paper IV

Thruster model for Observation Class Remotely Operated Vehicle

The paper presents the docking system for OCROV, and the autopilot created in Simulink. In the paper a model for the thrusters of the OpenROV is developed, based on tests done in a tank. A comparison of the model and the experimental results is performed and discussed.

The author performed most of the work in this paper.

Paper V

Variability assessment and forecasting of renewables: A review for solar, wind, wave and tidal resources

The paper is a review of the different renewable resources sun, wind, tide, and wave, in order to find variables that are common for forecasting the sources and assessing their variability. Tools are compared between the different sources and discussed.

The author took part in all the parts concerning wave power, and particularly in the study of the tools used to forecast wave energy.

8. Acknowledgment

This work is part of the OceaNET project, which is a multinational Initial Training Network (ITN) funded under the PEOPLE Programme (Marie Curie Actions) of European Union's FP7 under grant agreement no. 607656. I would like to thank all the managing team for this unique and fruitful experience.

Jens Engström, min huvudhandledare, tack för ditt stöd, din hjälp, och dina råd. Jag hoppas att de två kommande åren med dig kommer att bli ännu mer spännande och framgångsrika!

Johan Abrahamsson, min biträdande handledare, stort tack för dina råd och din tid, det är alltid trevligt att ha dig vid min sida på avdelningen. Magnus Rahm, tack för första året med dig, det var spännande att ha dig som handledare, jag hoppas du njuter ditt nya projekt! Rafael Waters, du är inte min handledare men nästan, så tusen tack för din hjälp i jobbet och din vänskap i livet.

Mats Leijon, jag vill tacka dig för att du välkomnade mig på avdelningen. Forskningsgruppen är trevlig och full av ambition, tack vare dig och din motivation.

Many thanks to you my office mates, Victor, Francisco, Dalina, Aya, Liguo, Simon, you make this office suuuuch a nice place, hope to have many more fika, dinners, and afterworks with you in the next years!

Thanks also to Kasper, Wei, Maria (and your mom!), Eduard, Liselotte, Ling, Johan F., Nicole, for the time we spent together around beers and cocktails in Uppsala, Lysekil, Stockholm, Hawai, New York, Aalborg..

Tobias, I will not thank you enough for all the time we spent in the lab, all the mistakes you fixed for me, all the components I burnt for you, all our walks in the cold between the lab and hallen… And thanks in advance for all the future help you will give me ☺

Of course I do not forget the OceaNET people, we had so great moments together, Nathalie, Michele, Boris, Yannick, Simon, FF, Mammad, Nicolas, Giovanni, Juan Carlos, FX, Cesc. Take care and hope to see you all in Lisboa next year!

Many thanks to Maria Nordengren, Anna Wiström, and Thomas Götschl. You are of great support and make my job so much easier here at Ångström.

Tusen tack also to the students who accepted to work with me on this exciting project! Johan Johansson, Ben Scheit, Sylvain Pourroy, Sophie Noiret.

I would like to thank the team who hosted me during those four months at IST in Lisboa, Antonio, Luis, Miguel, Jorge, Henrique, Pedro, and of course Filipa and Stephanie for the morning's coffees, lunches, surf sessions, and portuguese tips ☺

Mes soeurettes Hortense, Paulo, Cha, Malex, Loulette, je vous remercie pour votre soutien dans ce projet et dans la vie en géneral, vous êtes fantastiques ! Merci aussi à mes parents et beaux-parents qui m'accompagnent.

And last but not least, je veux remercier mon amour et fiancé Vincent Garcia, pour son soutien et son amour infaillibles, dans ma thèse comme dans la vie. Tu es une personne incroyable de force et de bonté, merci.

9. Svensk Sammanfattning

Remotely Operated Vehicles (ROVar) är undervattens robotar som styrs av människor och används för olika typer av operationer från enkla observationer till tunga jobb som borrning, kabelutläggning etc. De sistnämnda är dyra och kräver erfaren personal för att operera dem, samt båt för transport och kran med mera till sjösättning. Avdelning för elektricitetslära vid Uppsala universitet har i femton år utvecklat ett koncept av en vågenergiomvandlare som består av en boj och en linjär generator placerad på havsbotten. Flera vågkraftverk är kopplade till ett marin bottenställverk vars roll är att jämna ut effekten från de olika aggregaten och höja spänningsnivån till den som krävs i nätet.
Kabelkontaktering är en stor utmaning inom projektet eftersom vågkraftverken är små vilket gör att det krävs många enheter för att generera tillräckligt hög effekt. Nu för tiden är det dykare som utför den operation, men att använda OCROVar istället skulle vara ett intressant alternativ eftersom de är billigare och ganska enkla att styra. Kabelkontaktering är dock en tung arbetsuppgift och fordrar kraft som en OCROV inte har. Därför krävs det ett dockning system där farkosten kan ta sin kraft. Farkosten går till dockningpunkten, dockar, och kopplar kablarna med hjälp av en stödplatta.
Dockningproceduren måste utföras automatiskt för att det krävs en exakt omfördelning och snabb justering av farkostens rörelser.
En modell av en autopilot skapades i Matlab Simulink som består av tre enheter: orienterings, ROV, och positionerings enheterna. Den första justerar rörelsen av ROVn beroende på skillnaden mellan aktuella positionen och den planerade färdvägen. ROV enheten innehåller en kontrollenhet som anpassar propellerkraften till den som krävs för att nå önskad riktning och hastighet. Den innehåller också ROV modellen som beräknar nya ROV positionen och hastigheten. Sista enheten, som kallas positionering, består av ett Kalman filter som bedömer ROV positionen, och som ska användas i fallet att kommunikationen med positioneringssensorerna misslyckas eller fördröjs.
Autopilot modellen ska hanteras med ett positioneringssystem som använder grön laser och bildbehandling. Två gröna laserstrålar används som fixa punkter i bilden och från deras distans på bilden beräknas distansen mellan ROVn och dockningplattformen. Dessutom användas optisk odometri. Idén är att

mäta hur farkosten rör sig genom att titta på förändringen mellan två bilder från ROV kameran. Dessa två system, laser och odometri, ska användas tillsammans i syfte att få mer exakta resultat.
Lasersystemet har hitintills testats i luft. Distansmätningar gav intressanta resultat med mindre än 3% fel, och vinkelmätningar gav mindre än 10% fel för en distans av 1 meter. En fördel med det här systemet är att desto mer farkosten närmar sig dockningstationen, desto mer noggrant är systemet.
Utöver ROV projektet utfördes en review studie om variabilitet av vågenergi jämfört med andra energikällor såsom sol, vind, och tidvattenkraft. En analys av olika verktyg och modeller som används för att förutse dessa olika källor utfördes och hur man skulle kunna samla ihop dom och skaffa en enhetlighet i syfte att underlätta nätanslutning av flera olika energikällor.

10. References

[1] “CoE report 3_2 final.pdf.”.

[2] “capital-operating-and-maintenance-costs.pdf.” .

[3] G. E. Brown, “Operational considerations for underwater-mateable connectors,” in *OCEANS 2003. Proceedings*, 2003, vol. 4, p. 1843–1848 Vol.4.

[4] J. Cairns, “Recent Advances In Underwater Mateable Electrical Connectors,” in *OCEANS ’83, Proceedings*, 1983, pp. 507–511.

[5] D. Jenkins and M. Christiansen, “Enabling technology: High capacity wet mateable optic Connection,” in *2012 Oceans*, 2012, pp. 1–7.

[6] T. C. Galford and G. Purvinis, “A plea for the standardization of underwater connectors,” in *OCEANS’11 MTS/IEEE KONA*, 2011, pp. 1–6.

[7] R. D. Christ and R. L. W. Sr, *The ROV Manual, Second Edition: A User Guide for Remotely Operated Vehicles*, 2 edition. Amsterdam: Butterworth-Heinemann, 2013.

[8] R. Ekström and M. Leijon, “Control of offshore marine substation for grid-connection of a wave power farm,” *Int. J. Mar. Energy*, vol. 5, pp. 24–37, Apr. 2014.

[9] “Guidance and Control of Ocean Vehicles-Thor I Fossen.” [Online]. Available: https://www.scribd.com/doc/23822551/Guidance-and-Control-of-Ocean-Vehicles-Thor-I-Fossen. [Accessed: 29-Jul-2016].

[10] “Control Theory,” *Adlibris*, 01-Oct-2000. [Online]. Available: http://www.adlibris.com/se/bok/control-theory-9780748408788. [Accessed: 29-Jul-2016].

[11] P. Ridao, M. Carreras, D. Ribas, P. C. Abreu, and A. M. Pascoal, “4th IFAC Workshop onNavigation, Guidance and Controlof Underwater VehiclesNGCUV 2015Formation Control in the scope of the MORPH project. Part I: Theoretical Foundations★,” *IFAC-Pap.*, vol. 48, no. 2, pp. 244–249, Jan. 2015.

[12] P. Ridao, M. Carreras, D. Ribas, P. C. Abreu, M. Bayat, A. M. Pascoal, J. Botelho, P. Góis, J. Ribeiro, M. Ribeiro, M. Rufino, L. Sebastião, and H. Silva, “4th IFAC Workshop onNavigation, Guidance and Controlof Underwater VehiclesNGCUV 2015Formation Control in the scope of the MORPH project. Part II: Implementation and Results★,” *IFAC-Pap.*, vol. 48, no. 2, pp. 250–255, Jan. 2015.

[13] A. J. Häusler, A. Saccon, A. P. Aguiar, J. Hauser, and A. M. Pascoal, “9th IFAC Conference on Manoeuvring and Control of Marine CraftCooperative Motion Planning for Multiple Autonomous Marine Vehicles,” *IFAC Proc. Vol.*, vol. 45, no. 27, pp. 244–249, Jan. 2012.

[14] L. Wu, Y. Li, S. Su, P. Yan, and Y. Qin, “Hydrodynamic analysis of AUV underwater docking with a cone-shaped dock under ocean currents,” *Ocean Eng.*, vol. 85, pp. 110–126, Jul. 2014.
[15] F. Bonin-Font, G. Oliver, S. Wirth, M. Massot, P. Lluis Negre, and J.-P. Beltran, “Visual sensing for autonomous underwater exploration and intervention tasks,” *Ocean Eng.*, vol. 93, pp. 25–44, Jan. 2015.
[16] Y. Chen, X. Hu, D. Wang, H. Chen, C. Zhan, and H. Ren, “Researches on underwater transmission characteristics of blue-green laser,” in *OCEANS 2014 - TAIPEI*, 2014, pp. 1–5.
[17] B. Tian, F. Zhang, and X. Tan, “Design and development of an LED-based optical communication system for autonomous underwater robots,” in *2013 IEEE/ASME International Conference on Advanced Intelligent Mechatronics*, 2013, pp. 1558–1563.
[18] M. A. Rasyid and A. Budiyono, “Vision based distance measurement system using single laser pointer design for underwater vehicle,” *ResearchGate*, vol. 38, pp. 324–331, Oct. 2009.
[19] J. W. Giles and I. N. Bankman, “Underwater optical communications systems. Part 2: basic design considerations,” in *MILCOM 2005 - 2005 IEEE Military Communications Conference*, 2005, p. 1700–1705 Vol. 3.
[20] R. M. Pope and E. S. Fry, “Absorption spectrum (380–700 nm) of pure water II Integrating cavity measurements,” *Appl. Opt.*, vol. 36, no. 33, p. 8710, Nov. 1997.
[21] D. Scaramuzza and F. Fraundorfer, “Visual Odometry [Tutorial],” *IEEE Robot. Autom. Mag.*, vol. 18, no. 4, pp. 80–92, Dec. 2011.
[22] J. Mathew, A. K. Singh, Vinay A., A. S. Rao, V. S. Shekhar, A. K. C., K. N. B. Murthy, and S. Natarajan, “Proceedings of the 4th International Conference on Eco-friendly Computing and Communication SystemsFeature Extractionusing ORB-RANSAC for Face Recognition,” *Procedia Comput. Sci.*, vol. 70, pp. 174–184, Jan. 2015.
[23] “Wiley: RFID Handbook: Fundamentals and Applications in Contactless Smart Cards, Radio Frequency Identification and Near-Field Communication, 3rd Edition - Klaus Finkenzeller, Dörte Muller.” [Online]. Available: http://eu.wiley.com/WileyCDA/WileyTitle/productCd-0470695064.html. [Accessed: 29-Jul-2016].
[24] “Physics handbook for science and engineering av Carl Nordling, J Österman (Bok),” *Bokus.com*. [Online]. Available: http://www.bokus.com/bok/9789144044538/physics-handbook-for-science-and-engineering/. [Accessed: 31-Aug-2016].
[25] G. Benelli, A. Pozzebon, D. Bertoni, and G. Sarti, “An RFID-Based Toolbox for the Study of Under- and Outside-Water Movement of Pebbles on Coarse-Grained Beaches,” *IEEE J. Sel. Top. Appl. Earth Obs. Remote Sens.*, vol. 5, no. 5, pp. 1474–1482, Oct. 2012.
[26] S. Hasselmann, K. Hasselmann, E. Bauer, P. a. E. M. Janssen, G. J. Komen, L. Bertotti, P. Lionello, A. Guillaume, V. C. Cardone, J. A. Greenwood, M. Reistad, L. Zambresky, and J. A. Ewing, “The WAM model - a third generation

ocean wave prediction model.,” *ResearchGate*, vol. 18, pp. 1775–1810, Jan. 1988.
[27] N. Booij, R. C. Ris, and L. H. Holthuijsen, “A third-generation wave model for coastal regions: 1. Model description and validation,” *J. Geophys. Res. Oceans*, vol. 104, no. C4, pp. 7649–7666, Apr. 1999.
[28] F. Jose and G. W. Stone, “Forecast of Nearshore Wave Parameters Using MIKE21 Spectral Wave Model,” *ResearchGate*.
[29] “10082-portugal.pdf.” .
[30] “WMO702.pdf.” .
[31] “Thursters.” [Online]. Available: http://svseeker.com/rov_thrurters.htm. [Accessed: 17-Aug-2016].
[32] “Preliminary Propeller Efficiency Testing,” *OpenROV Forums*. [Online]. Available: https://forum.openrov.com/t/preliminary-propeller-efficiency-testing/1686. [Accessed: 17-Aug-2016].